Segmentation of megathrust rupture zones from fore-arc deformation patterns over hundreds to millions of years, Arauco peninsula, Chile

Daniel Melnick,[1] Bodo Bookhagen,[2,3] Manfred R. Strecker,[1] and Helmut P. Echtler[1,4]

[1] This work explores the control of fore-arc structure on segmentation of megathrust earthquake ruptures using coastal geomorphic markers. The Arauco-Nahuelbuta region at the south-central Chile margin constitutes an anomalous fore-arc sector in terms of topography, geology, and exhumation, located within the overlap between the Concepción and Valdivia megathrust segments. This boundary, however, is only based on ∼500 years of historical records. We integrate deformed marine terraces dated by cosmogenic nuclides, syntectonic sediments, published fission track data, seismic reflection profiles, and microseismicity to analyze this earthquake boundary over 10^2–10^6 years. Rapid exhumation of Nahuelbuta's dome-like core started at 4 ± 1.2 Ma, coeval with inversion of the adjacent Arauco basin resulting in emergence of the Arauco peninsula. Here, similarities between topography, spatiotemporal trends in fission track ages, Pliocene-Pleistocene growth strata, and folded marine terraces suggest that margin-parallel shortening has dominated since Pliocene time. This shortening likely results from translation of a fore-arc sliver or microplate, decoupled from South America by an intra-arc strike-slip fault. Microplate collision against a buttress leads to localized uplift at Arauco accrued by deep-seated reverse faults, as well as incipient oroclinal bending. The extent of the Valdivia segment, which ruptured last in 1960 with an M_w 9.5 event, equals the inferred microplate. We propose that mechanical homogeneity of the fore-arc microplate delimits the Valdivia segment and that a marked discontinuity in the continental basement at Arauco acts as an inhomogeneous barrier controlling nucleation and propagation of 1960-type ruptures. As microplate-related deformation occurs since the Pliocene, we propose that this earthquake boundary and the extent of the Valdivia segment are spatially stable seismotectonic features at million year scale.

1. Introduction

[2] Historical time-space records of great subduction earthquakes demonstrate that ruptures tend to occur repeatedly within distinct seismotectonic sectors along the fore-arc [e.g., *Ando*, 1975; *Kelleher*, 1972; *Lomnitz*, 1970; *Thatcher*, 1990]. Statistical analysis of such historical earthquake patterns have resulted in early attempts of assessing seismic hazard introducing the concept of "seismic gaps" [e.g., *Mogi*, 1979; *Thatcher*, 1990], and the time predictable model [*Shimazaki and Nakata*, 1980]. However, paleoseismic studies have shown that recurrence of large-magnitude earthquakes in subduction zones is variable and can exceed the time span of historical records [e.g., *Satake and Atwater*, 2007]. Because the magnitude of an earthquake largely depends on the fault area that ruptured and the amount of slip [e.g., *Hanks and Kanamori*, 1979; *Kanamori*, 1977; *Wells and Coppersmith*, 1994], understanding the factors that control lateral propagation of the dynamic earthquake rupture front, and the timescales on which seismotectonic segmentation is relevant, may furnish valuable information for our understanding of the earthquake process at plate boundaries and natural hazard assessment.

[3] Three major features have been proposed to control segmentation of subduction earthquake ruptures: bathymetric anomalies in the incoming oceanic plate [e.g., *Robinson et al.*, 2006; *Taylor et al.*, 1987], sediment thickness in the trench [*Ruff*, 1989], and discontinuities within the upper plate [e.g., *McCaffrey*, 1992; *Song and Simons*, 2003]. The extent of rupture segments also appears to be manifested by the spatial distribution of geophysical anomalies in fore-arc regions. For example, the positive correlation between subduction earthquake ruptures and the position and extent

[1]Institut für Geowissenschaften, Universität Potsdam, Potsdam, Germany.

[2]Department of Geological and Environmental Sciences, Stanford University, Stanford, California, USA.

[3]Geography Department and Institute for Computational Earth System Sciences, University of California, Santa Barbara, California, USA.

[4]GeoForschungsZentrum Potsdam, Potsdam, Germany.
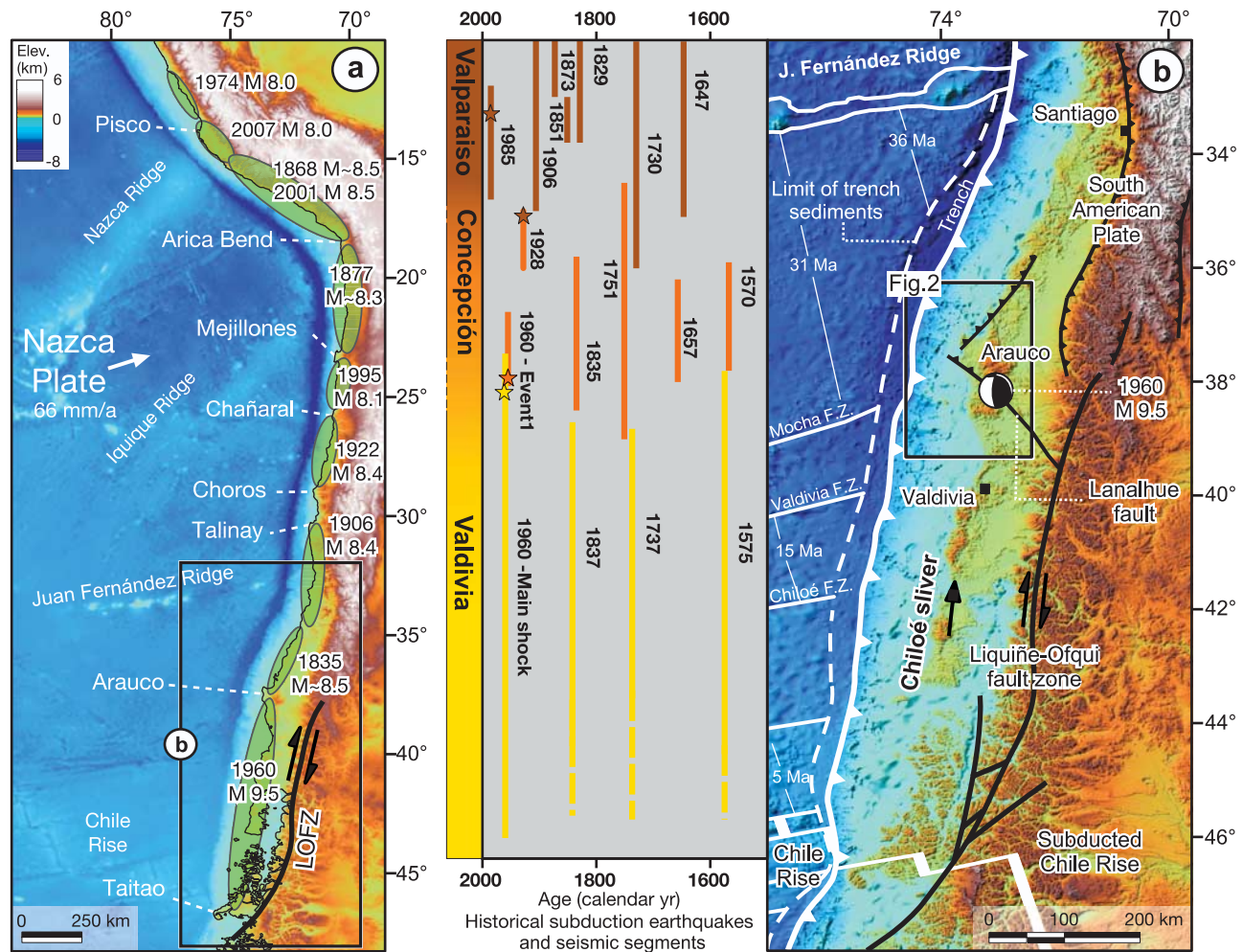
Figure 1. Index maps. (a) Major seismotectonic features of the central and south-central Andean fore-arc. Rupture segment of most recent, major ($M \geq 8$) subduction earthquake [*Beck and Ruff*, 1989; *Comte and Pardo*, 1991; *Lomnitz*, 1970, and references therein]. Note that distinct promontories seem to occur systematically at rupture segment boundaries. LOFZ, Liquiñe-Ofqui fault zone. (b) Location of the Arauco peninsula and study area. Major Quaternary faults compiled from references in text. Seismotectonic segments, rupture zones of historical subduction earthquakes, and main tectonic features of the south-central Andean convergent margin. Earthquake ruptures were compiled from *Campos et al.* [2002], *Comte et al.* [1986], *Kelleher* [1972], and *Lomnitz* [2004]. Dashed white line denotes edge of >1.5 km thick sediment fill in the trench. Data on Nazca plate and trench from *Bangs and Cande* [1997] and *Tebbens and Cande* [1997]. Segments of the Chile Rise subducted at 3 and 6 Ma from *Cande and Leslie* [1986].

of trench-parallel gravity anomalies at several subduction zones suggests that the segmentation of great earthquake ruptures is controlled by the structure acquired over timescales equivalent to the development of fore-arc basins, about $10^6 – 10^7$ years [*Llenos and McGuire*, 2007; *Song and Simons*, 2003; *Wells et al.*, 2003].

[4] Earthquake-related fore-arc deformation is usually recorded by coastal landforms, such as multiple levels of emerged abrasion platforms or coastal terraces. Detailed analysis of their geomorphic characteristics, chronology, and relation to the structural setting may provide valuable paleoseismic information, and can thus provide data needed to understand the long-term evolution of fore-arcs [e.g., *Lajoie*, 1986; *Taylor et al.*, 1987]. Interestingly, several studies have shown that distinct coastal landforms, like

peninsulas and embayments, tend to occur at seismotectonic boundaries [e.g., *Ando*, 1975; *Bourgois et al.*, 2007; *Collot et al.*, 2004; *Kelleher*, 1972; *Lomnitz*, 1970]. In fact, major historical seismotectonic segments along the Perú-Chile margin are delimited by such promontories, which mark distinct anomalies of the coastline (Figure 1a). Some of these earthquake boundaries also coincide with lower plate anomalies. For example, collision of the Peruvian Nazca Ridge (14°S) coincides with the Pisco peninsula and the boundary between the 1974 and 2007 M_w 8.0 ruptures; collision of the Chile Rise (46°S) correlates with the Taitao peninsula, which constitutes the southern limit of the 1960 M_w 9.5 earthquake rupture [*Cisternas et al.*, 2005; *Lomnitz*, 2004]. Conversely, there is no pronounced coastline anomaly or discrete earthquake rupture boundary in the regions
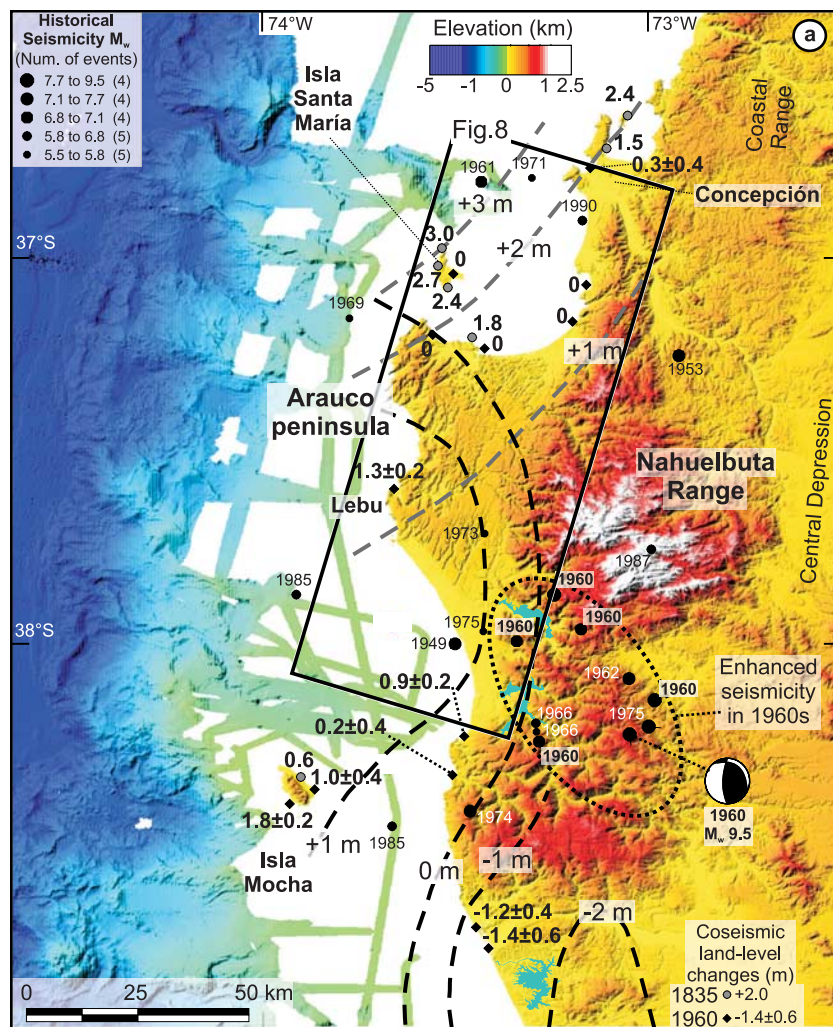
Figure 2a. Shaded topography (SRTM, NASA) merged with multibeam bathymetry from subduction Processes Off Chile (SPOC) cruise [*Reichert et al.*, 2002]. Historical M > 6 seismicity since 1950 [*Engdahl and Villaseñor*, 2002]; note cluster south of Nahuelbuta Range. Measurements and contours of coseismic land level changes from the 1960 [*Plafker and Savage*, 1970] and 1835 [*Darwin*, 1851] megathrust earthquakes.

where the Juan Fernández (32°S) and Iquique ridges (20°S) collide with the margin (Figure 1a), making unambiguous correlations between rupture segments and lower plate anomalies difficult. Indeed, some peninsulas that clearly correspond to historical earthquake rupture boundaries, like the Mejillones (23°S) and Arauco (38°S) peninsulas, apparently are not related to lower plate anomalies.

[5] In this study, we attempt to gain fundamental insight into the problem of earthquake rupture segmentation from a geological perspective and examine patterns of fore-arc deformation and exhumation over various temporal (10^2–10^6 years) and spatial (10^1–10^3 km) scales. This includes the analysis of coseismic land level changes during two great earthquakes of adjacent rupture segments, deformed Plio-cene-Quaternary marine sediments and terrace surfaces, and a synopsis of the late Cenozoic structural and thermal history. We focus on the south-central Chile margin (Figure 1b), where accounts of great earthquakes have been used to define historical seismic sectors [e.g., *Barrientos*, 1987; *Beck et al.*, 1998; *Campos et al.*, 2002; *Cisternas et al.*,

2005; *Comte et al.*, 1986; *Kelleher*, 1972; *Lomnitz*, 1970]. In particular, we address the evolution of the boundary between the Valdivia and Concepción segments. These fore-arc sectors lend themselves to a detailed analysis because of a rich array of deformed coastal landforms and syntectonic sedimentary sequences that allow a thorough analysis at various timescales. The boundary between these two segments is located at the Arauco peninsula (37.2–38.5°S), which forms a major anomaly along the Pacific margin of South America in terms of coastline morphology and trench-to-coast distance (Figure 1b). On the basis of historical records of subduction earthquakes spanning ~500 years, Arauco lies in the transition between two major and distinct seismic sectors, the Concepción and Valdivia seismotectonic segments (Figure 1b) [*Kaizuka et al.*, 1973; *Lomnitz*, 1970]. Structurally, the Arauco peninsula corresponds to a fore-arc high where the continental shelf has emerged to elevations above 400 m, resulting in the exposure of deformed Cenozoic marine rocks (Figures 2a and 2b). Uplifted and deformed marine terraces are also continuously
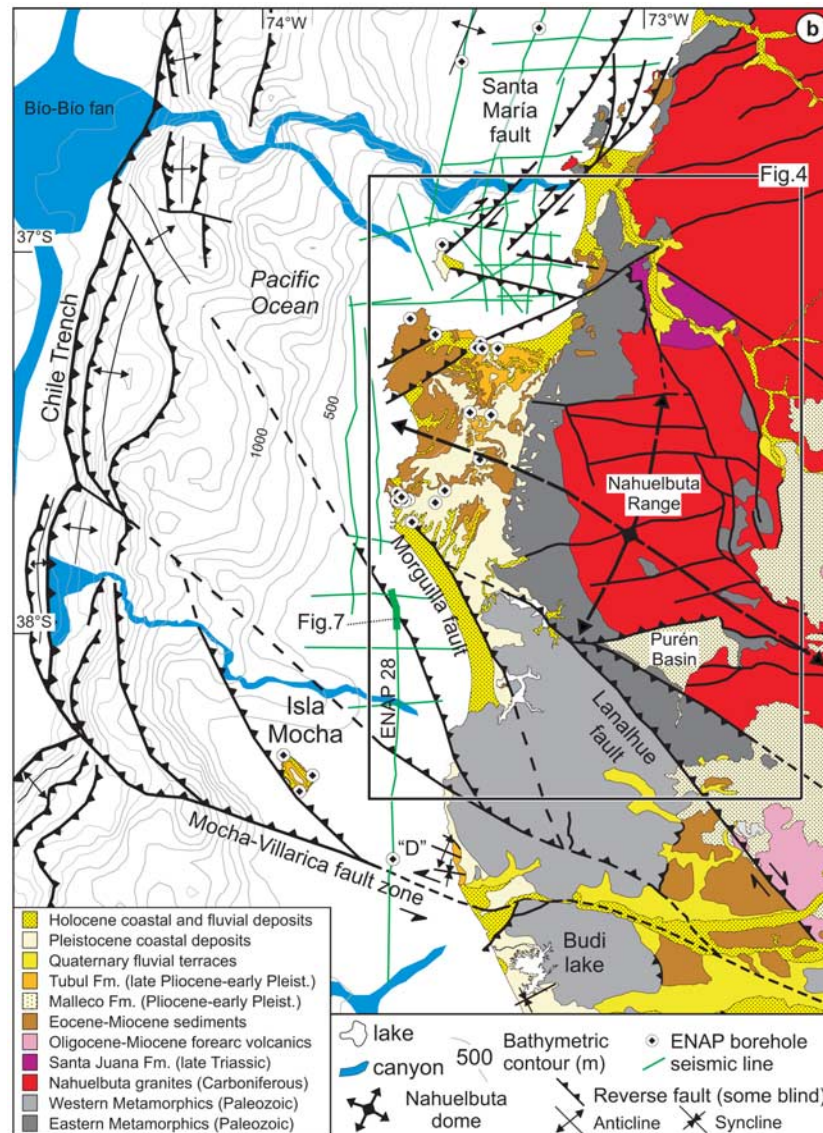
Figure 2b. Simplified geological map of the Arauco-Nahuelbuta region based on *Elgueta and Arcos* [1994], *Pineda* [1986], *Sernageomin* [2003], and our own mapping. Offshore structures interpreted from bathymetry and SPOC and ENAP seismic reflection profiles [*Melnick et al.*, 2006a]. Bathymetric contours from SPOC and Servicio Hidrográfico y Oceanográfico de la Armada (SHOA)-Chile data.

exposed along the coast of the peninsula. We use new geomorphic, seismic, borehole, stratigraphic, structural and geochronologic data, as well as results from various geophysical and geologic studies in the Arauco region [*Bohm et al.*, 2002; *Bruhn*, 2003; *Contreras-Reyes et al.*, 2008; *Glodny et al.*, 2008a, 2008b; *Haberland et al.*, 2006; *Hackney et al.*, 2006; *Krawczyk et al.*, 2006; *Lüth et al.*, 2003; *Melnick et al.*, 2006a; *Radic et al.*, 2005] to explore the control of fore-arc tectonics and inherited structures on the present-day segmentation of rupture propagation during a subduction earthquake. This also entails an overall evaluation of active plate boundary deformation and coastal landscape evolution on timescales spanning from 10^5 to 10^6 years. Furthermore, we analyze the regional tectonics of south-central Chile's fore and intra-arc regions to address whether the boundary between the Valdivia and

Concepción seismic segments is a transient or long-term feature.

2. Seismotectonic, Geologic, and Geomorphic Setting

2.1. Tectonics of the South-Central Chile Margin

[6] The Chile margin is formed by subduction of the oceanic Nazca plate under the South American continent at a convergence rate of 66 mm/a, which has decreased ∼40% over the last 10 Ma [*Kendrick et al.*, 2003]. The Nazca plate in the Arauco region is ∼32 Ma old, and its age increases continuously northward at ∼1 Ma/100 km along the trench (Figure 1b) [*Tebbens and Cande*, 1997]. The principal oceanic features are the Chile Rise, an active spreading center colliding with the margin at 46.5°S, and the Juan

Fernández Ridge, a hot spot seamount chain intersecting the margin at 33°S (Figure 1a). A major discontinuity of the Nazca plate in south-central Chile is the Valdivia Fracture Zone system at ∼40°S (Figure 1b), which separates oceanic crust generated at the Chile Rise to the south, from crust that formed at the East Pacific Rise to the north [*Tebbens and Cande*, 1997]. The Mocha Fracture Zone is subducted below the central part of the Arauco peninsula (Figure 1b). Multibeam bathymetry [*Reichert et al.*, 2002] images this Fracture Zone as two ∼5 km wide sharp and narrow ridges associated with several small seamounts. The bathymetric relief associated with the Mocha Fracture Zone amounts to a maximum of 1 km. Previous work has suggested that the anomalous uplift of the Arauco peninsula is a result of subduction of the Mocha Fracture Zone [*Boettcher*, 1999; *Cifuentes*, 1989; *Kaizuka et al.*, 1973; *Lohrmann et al.*, 2006; *Lomnitz*, 2004]. However, this fracture zone is oblique to the Pliocene-Quaternary plate convergence vector [*Somoza*, 1998], and thus its intersection with the margin has migrated southward at ∼100 km/Ma. Hence, its position below the Arauco peninsula has not been stationary. On the basis of our integrated data from this region, we will further address the role of the Mocha fracture in the seismotectonics of the region.

[7] A dramatic increase in sediment flux into the trench during the Pliocene caused by enhanced glacial erosion in the Patagonian Andes led to the onset of accretionary processes along the south-central Chile margin at that time [*Bangs and Cande*, 1997]. Seismic profiles image 1.5–2.3 km of glacially derived sediments in the trench, a relatively narrow (∼30–40 km) and young (∼2–3 Ma) frontal accretionary wedge, and an up to 1.5 km thick subduction channel [*Bangs and Cande*, 1997; *Contreras-Reyes et al.*, 2008]. Cenozoic fore-arc basins exist over most of the Chile margin and are filled with more than 3 km of sediments in the shelf region [e.g., *González*, 1990]. Seismic reflection profiles and coastal exposures reveal that fore-arc basins between 34 and 45°S record Miocene to early Pliocene extension, followed by contraction since the late Pliocene [*Melnick and Echtler*, 2006a]. This change in kinematics is interpreted to have been caused by the shift from erosive to accretionary conditions after glacial age filling of the Chile trench.

[8] The onshore part of the margin consists of (Figures 2a and 2b) [e.g., *Melnick and Echtler*, 2006b; *Mpodozis and Ramos*, 1990] (1) the Coastal Platform, formed by uplifted Cenozoic marine and coastal sequences, the focus of this study; (2) the Coastal ranges, which include a segmented Permo-Triassic accretionary complex and a late Paleozoic magmatic arc; (3) the Central Depression, a low-relief area formed by Oligo-Miocene sedimentary and volcanic rocks covered by Pliocene-Quaternary fluvial-alluvial sediments; and (4) the Main Cordillera, which hosts a long-lived Meso-Cenozoic magmatic arc and intra-arc volcano-sedimentary basins.

[9] The principal structural feature of the Main Cordillera is the Liquiñe-Ofqui fault zone (LOFZ; Figure 1b), a dextral strike-slip system that controls the architecture of the intra-arc region between the Chile Triple Junction at 46.2°S and the Copahue volcano at 38°S [e.g., *Hervé*, 1994; *Lavenu and Cembrano*, 1999; *Rosenau et al.*, 2006]. The LOFZ decouples a fore-arc sliver from the rest of the continent, the Chiloé block (Figure 1a) [*Beck et al.*, 1993; *Forsythe and Nelson*, 1985; *Lavenu and Cembrano*, 1999], which moves northward with respect to the stable Andean foreland to the east (Figure 1b). Kinematic modeling of the LOFZ predicts a long-term (∼6 Ma) shear rate of 32 ± 6 mm/a in a southern domain (46–42°S), which decreases to 13 ± 3 mm/a for a northern domain (42–38°S) [*Rosenau et al.*, 2006]. This velocity gradient may have been partly accommodated by internal deformation of the Chiloé fore-arc sliver, consistent with Pliocene-Quaternary contractional and transpressional structures that strike oblique to the margin [*Melnick and Echtler*, 2006a, 2006b; *Rosenau et al.*, 2006]. The development of these structures and their role in accommodating sliver motion is further documented by shortening in the Arauco region as shown in this study. Dextral shear along the LOFZ increased at ∼6 Ma, as evidenced by isotopic dating of synkinematic minerals in high-strain mylonites [*Cembrano et al.*, 2002] and onset of rapid exhumation driven by transpression [*Thomson*, 2002]; this acceleration has been interpreted as a result of the consecutive collision of three segments of the Chile Rise in the region between 47.5 and 46.5°S (Figure 1b). The long-term strike-slip rate of the LOFZ predicted by kinematic modeling may have slowed down, because the present margin-parallel component of oblique plate convergence is only 24 mm/a according to geodetic data [*Kendrick et al.*, 2003] or 28 mm/a according to the NUVEL-1a global plate motion model [*Demets et al.*, 1994]. This decrease in slip rate along the LOFZ is likely a result of the continuous decline in overall plate convergence rate [*Kendrick et al.*, 2003]. Global Positioning System (GPS) data shows northward, margin-parallel velocities that reach 6.8 mm/a in the southern sector of the Chiloé sliver (45–43°S), accounting for ∼30% of the margin-parallel component of oblique convergence [*Wang et al.*, 2007]. These regional GPS data show margin-parallel translation of the Chiloé sliver and dextral strike-slip motion of the LOFZ. Unfortunately, no estimates of slip rates along the LOFZ on shorter timescales of 10^3–10^5 years have been obtained so far.

[10] Contemporary deformation in the central and southern region of the Chiloé sliver (45–39°S) still includes postseismic relaxation following the 1960 M_w 9.5 earthquake, in addition to interseismic strain accumulation [*Klotz et al.*, 2001; *Wang et al.*, 2007]. This postseismic signal is no longer visible in the northern leading edge of the Chiloé sliver, which corresponds to the southern Arauco region, where GPS data document counterclockwise rotations in addition to interseismic coupling [*Moreno et al.*, 2008].

2.2. Cenozoic Geology of the Arauco Fore-Arc Basin and Nahuelbuta Coastal Range

[11] The Arauco Basin contains over 3 km of late Cretaceous to Holocene continental and marine sediments, and has been a major center of coal mining and hydrocarbon exploration for over a century. This depocenter includes the Campanian to Maastrichtian Quiriquina Formation, the Paleocene to Eocene synextensional Lebu Group, the late Miocene to early Pliocene synextensional Ranquil Formation, and the late Pliocene to Pleistocene syncontractional Tubul Formation [e.g., *Biró*, 1979; *Elgueta and Arcos*, 1994; *Encinas et al.*, 2008; *Finger et al.*, 2007; *Le Roux and Elgueta*, 1997; *Melnick and Echtler*, 2006a; *Pineda*,
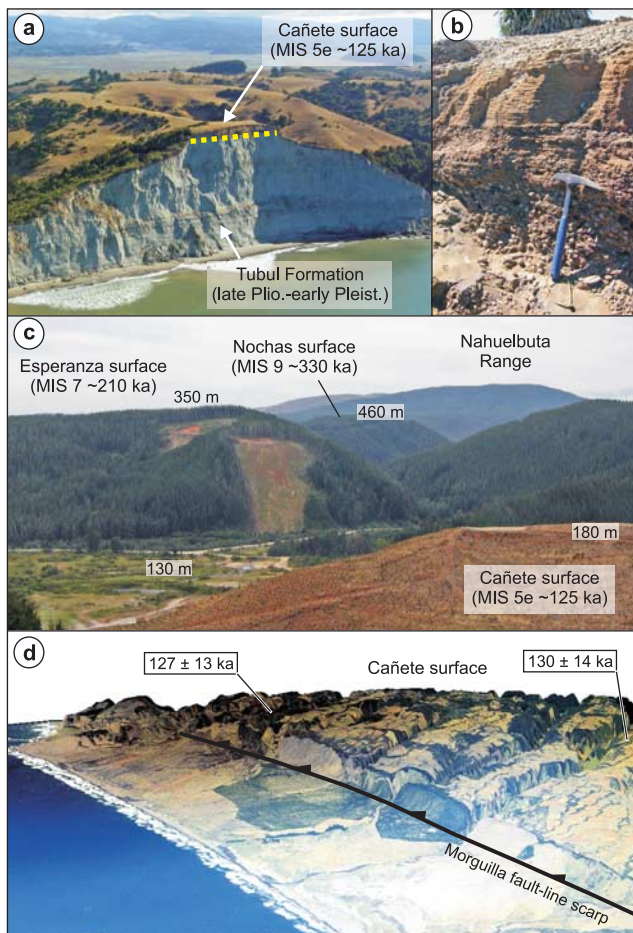
Figure 3. Field views of the Arauco peninsula. (a) Aerial view to the south of the Tubul Formation and Cañete surface near the town of Tubul, northern edge of the peninsula. The dashed yellow line shows the base of the Cañete Formation underlying the Cañete surface. (b) Typical quartzitic fluvial conglomerate of the Cañete Formation sampled for cosmogenic nuclide dating. (c) View to the east of the three emerged marine terraces in the center of the peninsula near Curanilahue. (d) Aerial photo draped over digital elevation model illustrating the Morguilla fault scarp and the dissected Cañete surface at the southwestern edge of the peninsula. Sampling sites and cosmogenic nuclide ages indicated (data in Table 1).

1986] (Figure 2b). During Miocene to early Pliocene time, low amounts of trench fill and high plate convergence velocity caused subduction erosion resulting in over 1.5 km of fore-arc subsidence and synextensional deposition of the Ranquil Formation, comprising mainly lower bathyal turbidites [*Encinas et al.*, 2008; *Finger et al.*, 2007; *Melnick and Echtler*, 2006a]. During the shift toward accretionary conditions between 4.5 and 2.5 Ma, positive inversion and uplift of fore-arc depocenters occurred in the region between 34 and 45°S [*Melnick and Echtler*, 2006a]. Growth strata associated with seismically active reverse faults reflect continuous and ongoing shortening and uplift coeval with the deposition of the Tubul Formation [*Melnick et al.*, 2006a].

[12] The Nahuelbuta Range is located immediately east of the Arauco peninsula and has a dome-like morphology with a maximum elevation of 1525 m. Considering the elevations of the Coastal Cordillera, which are typically well below 700 m, Nahuelbuta is an anomalous sector in term of topography (Figures 1b and 2a). This range is formed by a Carboniferous granitic core bounded by high-temperature contact metasedimentary rocks referred to as the Eastern Series [*Hervé*, 1988]. The northwest-striking Lanalhue fault running along the southern flank of Nahuelbuta (Figure 2b) marks the contact between the Eastern and Western Series, which consist of high-pressure and low-temperature metasedimentary rocks and ophiolitic components [*Hervé*, 1988]. Dating of synkinematic minerals in mylonitic shear zones of the Lanalhue fault indicate sinistral shear at ~275 Ma [*Glodny et al.*, 2008a]. Counterparts of the Nahuelbuta granite crop out at 39.5°S in the Main Cordillera, leading these authors to correlate these outcrops and propose ~100 km of sinistral displacement along the Lanalhue fault during Permian time.

[13] However, the Lanalhue fault also cuts fluvial and alluvial terraces of the Malleco Formation on the eastern flank of the Coastal Cordillera (Figure 2b), whose age range is bracketed by several 4.4 ± 0.5 to 0.8 ± 0.3 Ma old volcanic deposits interbedded near the base and top, respectively, of the predominantly clastic sequence [*Suárez and Emparán*, 1997]. The The Incoming Plate to MegaThrust EarthQuake Processes (TIPTEQ)-North local seismic network [*Haberland et al.*, 2006] registered several clusters of crustal earthquakes between 1 and 22 km depth, exactly below the surface expression of the Lanalhue and Morguilla faults. The latter seems to be a trenchward continuation of the Lanalhue fault, cutting through the southern flank of the Arauco peninsula where it offsets the Pleistocene Cañete surface (Figures 2b and 3d). Focal mechanisms are consistent with steeply dipping fault planes as expected also from linear fault scarps, as observed in outcrops near the town of Capitán Pastene, and as imaged by the TIPTEQ deep seismic reflection profile shot at 38.2°S [*Groß et al.*, 2008]. These geophysical and geological data identify the Lanalhue fault as a steeply NE-dipping, long-lived crustal-scale structure with neotectonic activity manifested by deformed Quaternary landforms and localized crustal seismicity.

[14] Fission track (FT) cooling ages from the Nahuelbuta Range and adjacent sectors of the Coastal Cordillera have been reported in a regional thermochronologic survey of south-central Chile [*Glodny et al.*, 2008b]. At Nahuelbuta, nine mean apatite FT ages range from 106 ± 29 to 54.6 ± 4.1 Ma and seven mean zircon FT ages of paired samples range from 242 ± 29 to 179 ± 49 Ma (Figures 4a and 4b). Inverse modeling of track length distribution data of four apatite FT samples from the top of the Nahuelbuta Range (samples at higher elevations in Figure 4a) indicates slow Tertiary cooling at an exhumation rate of $0.03-0.04$ mm/a until 4 ± 1.2 Ma, and an increase to >0.2 mm/a since that time [*Glodny et al.*, 2008b]. In contrast, modeling of samples from the Valdivia and Concepción regions located farther south (39–40°S) and north (36–37°S) of Nahuelbuta, respectively, do not show this increase in cooling during the early Pliocene, but exhibit a rather slow continuous cooling trend corresponding to an exhumation rate of
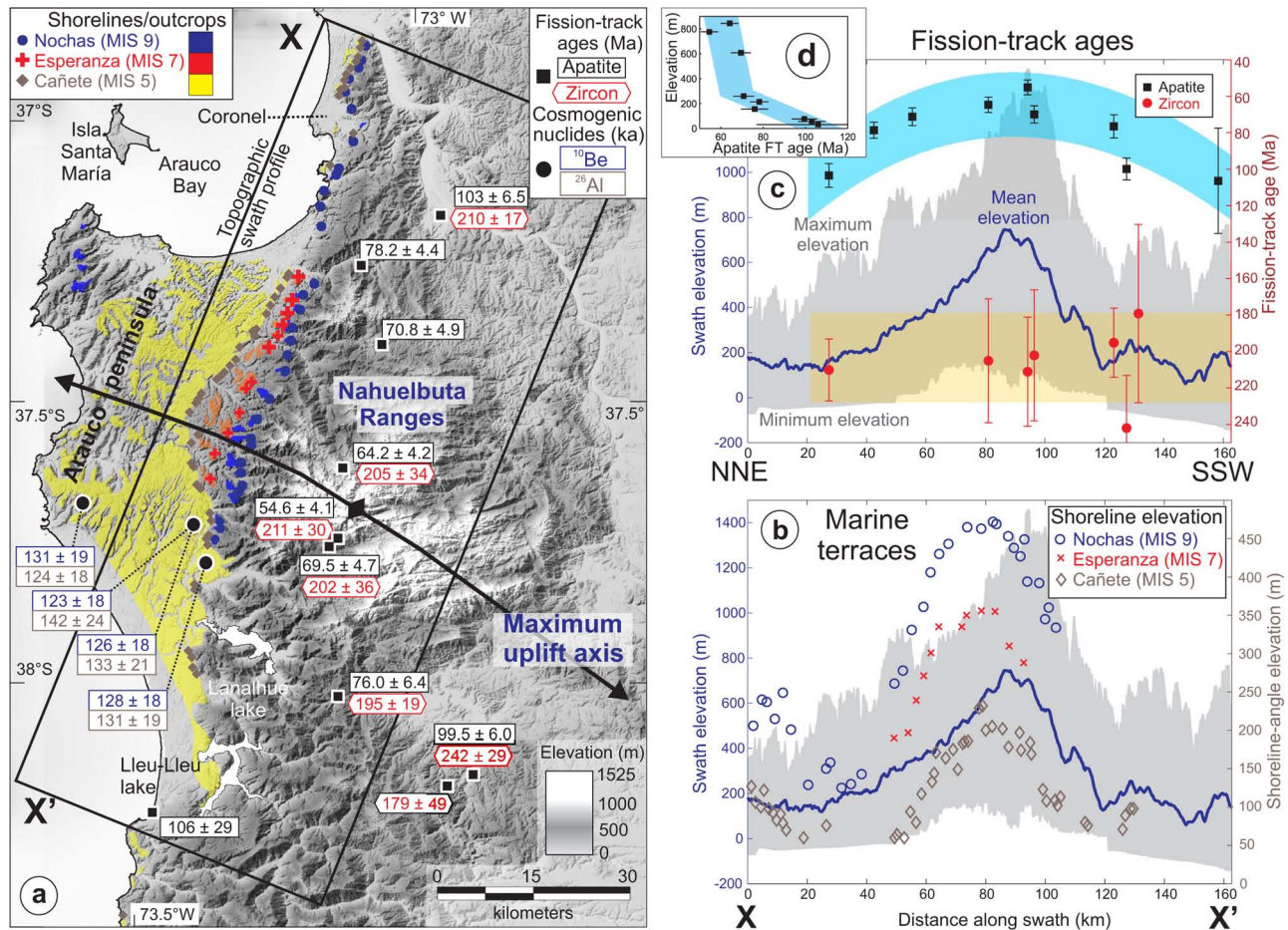
Figure 4. Markers of uplift and deformation. (a) Map of marine terraces in the Arauco region and location of shoreline angle measurement. Cosmogenic nuclide ages of the Cañete terrace are shown. Zircon and apatite fission track (FT) ages from *Glodny et al.* [2008b]. (b) Topographic swath profile, area shown in Figure 4a, and elevation of shoreline angles projected to the profile. (c) FT ages projected along the same profile. Note the similar warping pattern between terrace shorelines, topography, and apatite FT ages. In turn, zircon FT ages have a flat pattern. (d) Age-elevation plot of apatite FT ages. The inverse relation implies that more exhumation has occurred in the higher-elevation region.

0.03–0.04 mm/a over the past ∼100 Ma. This latter rate can be considered as the long-term regional background exhumation rate along the Coastal Cordillera of south-central Chile, except for Nahuelbuta.

2.3. Quaternary Geomorphic Setting of the Arauco-Nahuelbuta Region

[15] Only a few previous studies have focused on the tectonic geomorphology of this region and addressed the relation between late Quaternary and historic fore-arc deformation. The pioneer work of *Kaizuka et al.* [1973] described three sequences of uplifted marine terraces at Arauco including the well preserved Cañete surface correlated with marine oxygen isotope stage (MIS) 5e that reaches 232 m and which has been inferred to correlate with MIS 5e, as well as two higher surfaces, Esperanza and Nochas, which reach 360 and 471 m, respectively (Figures 3c and 4b). These three surfaces are abrasion platforms covered by a veneer of shallow marine, fluvial, and eolian sediments. The marine surfaces are folded around a northwest-trending anticline in the center of the

peninsula (Figures 4a, 4b, and 6c). Our analysis of terrestrial cosmogenic nuclides corroborates a last interglacial (MIS 5e) origin for the Cañete surface (Table 1; sample sites shown on Figures 3a, 3d, 4a, and 5; see sections 3 and 4.3 and auxiliary material for details).[1] A marked lower surface exists at the southwestern edge of Arauco near Lebu where it reaches a maximum elevation of 125 m. This surface has marine and eolian deposits comparable to the higher surfaces, and was probably formed during one of the interstadial stages of the last glacial period. However, because of its limited extent along the coast, this terrace is less suitable to explore margin-parallel variability of tectonic uplift.

[16] The Nahuelbuta Range has a domal morphology forming a major regional drainage anomaly along south-central Chile's Coastal Cordillera [*Rehak et al.*, 2008]. Several higher, barren surfaces of inferred marine abrasion origin exist up to about 1000 m elevation on the western

---

[1]Auxiliary materials are available in the HTML. doi:10.1029/2008JB005788.

Table 1. Cosmogenic Nuclide Ages of the Cañete Surface

Sample Name	Elevation (m above sea level)	Sample Depth (m)	^{10}Be (10³ atoms/g)[a]		^{26}Al (10³ atoms/g)[a]		$^{26}Al/^{10}Be$		^{10}Be Model Age (ka)[b]		^{26}Al Model Age (ka)[b]		Mean Model Age (ka)	
			Measured Value	Associated Error	Measured Value	Associated Error	Measured Value	Associated Error	Measured Value	Associated Error	Measured Value	Associated Error	Measured Value	Associated Error
Ar08	50	1.5	133.06	3.73	858.23	61.15	6.4	0.5	126	18	133	21	130	14
Ar08	50	2.1	72.93	2.19	519.48	50.37	7.1	0.7	123	18	142	24	133	14
Ar05	61	1.8	101.40	2.99	639.31	23.35	6.3	0.3	128	18	131	19	130	13
Ar07	150	0.7	340.46	8.25	1934.15	52.15	5.7	0.2	131	19	124	18	127	13

[a]Uncertainties in atomic abundances (1σ) only represent errors associated with the accelerator mass spectrometry (AMS) ratio measurements. We did not include the 1σ uncertainty in the Be carrier addition (∼2%) and stable AMS measurements (∼5%). These results are corrected for ratios measured in process blanks as described in the text.

[b]Calculated by using corrected production rates scaled to site-specific altitudes [*Lal*, 1991] and depth shielding based on spallation, fast muons, and negative muon capture [*Granger and Muzikar*, 2001; *Granger and Smith*, 2000]. We used a density of 1.8 g/cm³ and attenuation length of 160 g/cm². Uncertainties in depth-shielded ages are fully propagated from AMS uncertainties and do include a 10% 1σ uncertainty in nuclide production rates including scaling factors for altitude and latitude, as well as 10% 1σ uncertainties in density, attenuation coefficients, and half-lives. No uncertainties are propagated for depth shielding because no uncertainties are provided for coefficient by *Granger and Smith* [2000].

flank of the Nahuelbuta Range. Several faults of unknown kinematics, but with clear morphological expression form a curved array that follows the topography along the eastern flank of the Nahuelbuta Range (Figure 2b). Some of these faults juxtapose Triassic sediments with Paleozoic intrusives and control the occurrence of several metamorphic roof pendants, and may thus have formed prior to the Cenozoic. The Purén Basin is a triangular intermontane depression at the southern flank of Nahuelbuta, which is filled with Plio-Quaternary sediments of the Malleco Formation. This basin is limited by two NW- and SW-dipping reverse faults that splay from the Lanalhue fault (Figure 2b). The northern fault juxtaposes Paleozoic intrusives and Malleco sediments and has a clear morphological expression with pronounced triangular facets suggesting a Quaternary age.

[17] The Lanalhue and Lleu-Lleu lakes are located in the southern sector of the Arauco peninsula and immediately farther south of it, respectively (Figure 4a). These coastal lakes are drowned fluvial valleys located in the hanging wall of the Morguilla fault. It is likely that tectonic defeat associated with slip on the Morguilla fault and resulting uplift of its hanging wall and possibly tilting at the edge of the Arauco anticline resulted in the formation of both lakes. A high-resolution seismic survey combined with sediment coring revealed the original fluvial nature of these lakes and the post-MIS 5e flooding and uplift history [*Blumberg et al.*, 2007].

[18] Pleistocene sedimentary units and coastal landforms are also abundant in the neighboring regions of the Arauco Peninsula. On Isla Santa María, 12 km to the north (Figure 2a), marine and eolian sediments crop out in vertical sea cliff exposures. Radiocarbon dating of paleosol horizons interbedded in the marine-dominated sequence, which represent markers of paleo sea-level position, indicate deposition between 53 and 27 ka, corresponding to uplift at an average rate of 1.8±0.4 mm/a [*Melnick et al.*, 2006a]. Sequences of uplifted Holocene beach berms are exposed in a coastal plain in the eastern part of the island. Beach berms are also found on the surroundings of the Arauco Gulf and on Isla Mocha, ∼60 km south of Arauco (Figure 2a) [*Kaizuka et al.*, 1973; *Nelson and Manley*, 1992]. *Bookhagen et al.* [2006] calculated a maximum uplift rate of 2.3 ± 0.1 mm/a over the past ∼3 ka for Isla Santa María on the basis of luminescence ages of beach berm crests. In their detailed study of uplifted strandlines at Isla Mocha, *Nelson and Manley* [1992] reported uplift rates between 5.5 and 10 mm/a over the past ∼11 ka on the basis of radiocarbon dating of marine shells.

[19] The Santa María and Mocha islands as well as the core of the Arauco peninsula are tilted eastward (Figure 6c). In a previous study, we showed that Isla Santa María consists of two asymmetrically tilted Pleistocene surfaces, which represent the forelimbs of two anticlines that converge at the island and are cored by reverse faults [*Melnick et al.*, 2006a]. At Isla Mocha northeastward tilting is evident from inclined marine surfaces in the central ridge of the island, a pronounced asymmetry in the drainage system, as well as from the two measurements of coseismic uplift made by *Plafker and Savage* [1970] after the 1960 earthquake (Figure 2a). Short-wavelength tilting at Isla Mocha is also possibly linked to a major reverse structure, the Mocha-
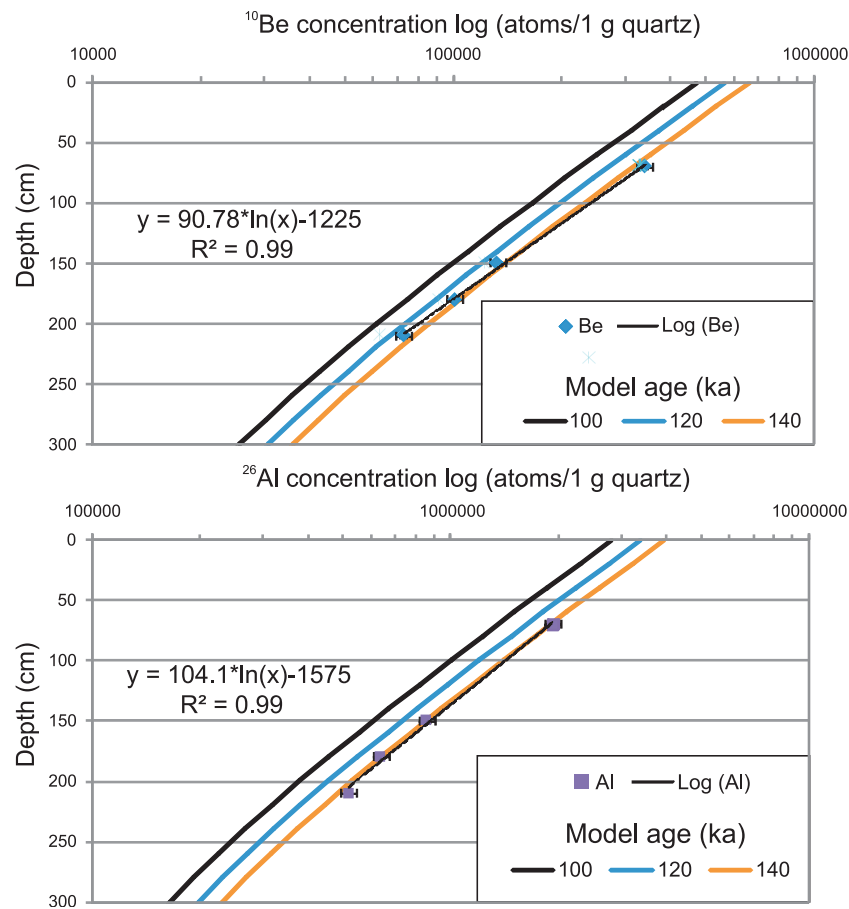
Figure 5. Cosmogenic nuclide composite depth profiles and age models for (top) [10]Be and (bottom) [26]Al. Curves for 100, 120, and 140 ka model ages are shown. See text for methods and details. Sampling locations are shown in Figure 4a. The composite profile includes four samples collected at three sites.

Villarica fault zone [*Melnick and Echtler*, 2006b], which cuts through the entire margin from the trench to the Main Cordillera (Figure 2b).

2.4. Historic Subduction Earthquakes in the Arauco Region

[20] Historical records of great earthquakes in Chile of the ultimate ~500 years reveal that the Arauco peninsula is located in the transition between the Valdivia and Concepción seismotectonic segments (Figure 1b) [*Kaizuka et al.*, 1973; *Lomnitz*, 2004]. The Valdivia segment ruptured last during the 1960 M_w 9.5 earthquake, while the last great event that nucleated in the Concepción segment occurred in 1835 with an estimated magnitude of 8.5 [*Lomnitz*, 2004]. It appears from the spatiotemporal trends of ruptures in these two segments that great earthquakes occur in pairs, probably triggered by stress transfer mechanisms that load the neighboring sector [e.g., *Freed*, 2005]. However, this does not seem to be the case for the transition between the Concepción and Valparaiso segments farther north, which appear to have a rather diffuse boundary both in space and time (Figure 1b).

[21] The 1960 earthquake sequence started with four foreshocks reaching up to M_w 8.2, followed a day after by the M_w 9.5 main shock and a major M_w 7.9 aftershock [*Cifuentes*, 1989; *Engdahl and Villaseñor*, 2002; *Kanamori*,

1977]. All these large-magnitude events occurred on 21 and 22 May and nucleated along a discrete, NW−SE elongated region between 38.8° and 38.2°S, at approximate depths of 35−50 km (Figure 2a). This elongated region, whose shape is independent of relative relocation uncertainties, is parallel to the Lanalhue fault and remained the locus of sustained seismic activity with earthquakes up to M_w 7.9 until the mid 1970s [*Engdahl and Villaseñor*, 2002]. Coseismic uplift caused by the 1960 events of 1.5 m was registered immediately after at Lebu [*Alvarez*, 1963]; at the same locality *Plafker and Savage* [1970] measured 1.3 ± 0.2 m in 1968 (Figure 2a). No clear evidence of coastal land level changes was found north of Lebu suggesting that rupture did not propagate beyond the Arauco peninsula. This assessment is also supported by repeated leveling of a line running along the inland region that recorded no more than 11 cm of uplift between the pre- and postearthquake surveys [*Plafker and Savage*, 1970]. Uplift of 1.7 m was measured immediately after the earthquake at Isla Mocha [*Seivers*, 1963] and later of 1.8 ± 0.2 and 1.0 ± 0.4 m at the western and eastern coast, respectively, by *Plafker and Savage* [1970] in 1968, suggesting some landward tilting. Immediately east of Mocha uplift was only 0.9 ± 0.2 and 0.2 ± 0.4 m (Figure 2a). South of 38.5°S, 1960 land level changes along the coastline were dominated by subsidence, which reached 2.7 m near the city of Valdivia at 40°S [*Plafker and Savage*, 1970].
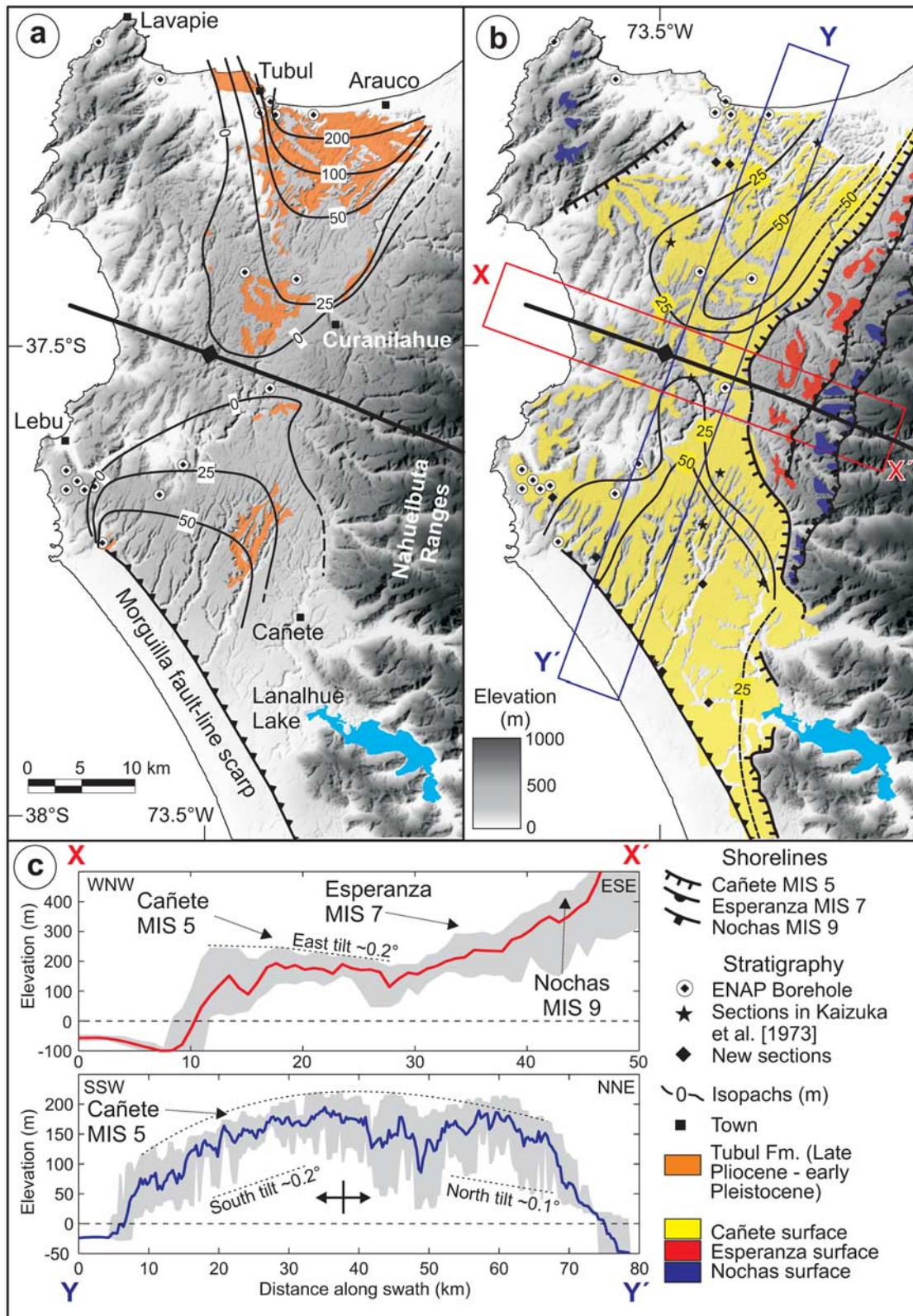
Figure 6. Syntectonic sediments. (a) Outcrops and isopachs of the Tubul Formation (late Pliocene to early Pleistocene) based on 17 boreholes and field exposures. (b) Outcrops and isopachs of the Cañete Formation (MIS 5e, ~125 ka) derived from boreholes and indicated field exposures. Shorelines and outcrops associated with the Esperanza and Nochas surfaces are also shown. (c) Swath topographic profiles along and across the axis of the Arauco anticline. Areas of profiles shown in Figure 6a.

Table 2. Pleistocene Deformation Rates Derived From Marine Terrace Data

Terrace Name	MIS	Age (ka)	Error (ka)	Sea Level Elevation[a] (m)	Sea Level Elevation Error (m)	Shoreline Angle Error[b] (m)	Maximum Uplift Rate (mm/a)	Maximum Uplift Rate Error (mm/a)	Shortening Rate (mm/a)	Shortening Rate Error (mm/a)
Cañete	5e	125	10	5	3	5	1.8	0.2	5.59	0.17
Esperanza	7	210	10	−3	4	10	1.7	0.2	6.17	0.3
Nochas	9	330	10	4	4	15	1.4	0.2	6.23	0.25

[a]Sea level elevation at the respective marine oxygen isotope stage.
[b]Estimated error in measurements of shoreline angle elevations of each terrace.

[22] Coseismic uplift during the 1835 earthquake was measured by Darwin and FitzRoy in the Arauco Bay area and at Isla Mocha about two to four weeks after the event [Darwin, 1851]. Maximum uplift of 3.0 m occurred at Isla Santa María, 2.4 m at Isla Quiriquina in the Bay of Concepción, 1.8 m at Tubul and 1.5 m at the harbor of Talcahuano, whereas Isla Mocha rose only by 0.6 m (Figure 2a).

[23] Isobases of coseismic uplift from the 1960 and 1835 earthquakes seem to converge at the Arauco peninsula (Figure 2a), similar to rupture zones of previous earthquakes in south-central Chile (Figure 1a) [Lomnitz, 1970, 2004]. These events led Lomnitz [1970] to define the Valdivia and Concepción seismic segments and subsequently led Kaizuka et al. [1973] to propose that emergence of the Arauco peninsula occurred by accumulated coseismic uplift during both Valdivia- and Concepción-type earthquakes. This would imply that at least some permanent deformation in this region, where two distinct rupture segments overlap, is accumulated during the coseismic phase of the seismic cycle. We further explore this hypothesis by examining the spatial distribution of Neogene sediments exposed at Arauco and patterns of deformed Quaternary marine terraces, and by comparing them with coseismic uplift patterns from the 1835 and 1960 earthquakes.

3. Methods

[24] Our study of seismotectonic processes is based primarily on geological, geomorphic, and structural field mapping. We used air photos at scales of 1:20,000 to 1:125,000 and digital elevation models derived from shuttle radar topography mission (SRTM) data [Farr et al., 2007], digitized topographic maps at 1:50,000 scale, and ASTER satellite imagery. Offshore industry seismic reflection profiles (Figure 2b) made available by Empresa Nacional del Petróleo (ENAP, Chile's state oil company) were integrated with onshore structural and sedimentological observations [e.g., Melnick and Echtler, 2006a; Radic et al., 2005]. Isopach maps of late Pliocene and Pleistocene units were generated from 17 ENAP exploration boreholes (see auxiliary material, Table S1) [Elgueta and Arcos, 1994]; in addition to seven exposed stratigraphic sections originally surveyed by Kaizuka et al. [1973] and revisited during our study, as well as seven new stratigraphic sections surveyed in the present study. Interpolated isopach contours were derived using the subsurface data in addition to the distribution of outcrops at the surface and their dip angles (Figures 6a and 6b).

[25] We measured the elevation of three uplifted Pleistocene marine terraces to understand deformation patterns and to calculate surface uplift rates in the Arauco region (Figures 3c, 4a, and 4b). Worldwide, the best morphologically expressed marine terrace dates from the last interglacial sea level highstand (MIS 5e) [e.g., Hearty and Kindler, 1995; Johnson and Libbey, 1997]. The age of MIS 5e is arbitrarily fixed to range from 130 to 116 ka [Kukla et al., 2002], but may extend between 134 and 113 ka [Muhs et al., 2002], with a peak from 128 to 116 ka on tectonically stable regions, where it is found at elevations of 2–8 m [Muhs, 2002]. Other well-represented interglacial terraces worldwide are from MIS 7 and 9, with age ranges of 200–220 and 320–340 ka, respectively (Table 2) [e.g., Chappell and Shackleton, 1986; Marquardt et al., 2004; Shackleton et al., 1990; Shackleton and Opdyke, 1973].

[26] Marine terraces can be used as markers of paleo sea-levels. The elevation of the shoreline angle, the base of the paleo sea cliff, is considered most representative of relative eustatic sea level highstands correlated with odd-numbered MIS [e.g., Keller and Pinter, 2002; Lajoie, 1986]. Shoreline angles of the three preserved terraces in the Arauco region were measured at 93 locations (Figure 4a). On the terraces of the Arauco peninsula, it is assumed that the present-day elevation of the mantled material closely approximates former mean sea level elevation. However, in some cases this assumption incorporates an additional uncertainty, because younger eolian or colluvial material may cover the surface. However, we could discard this possibility at many localities where the abrasion surface was still visible. Despite this, a conservative error of 5, 10, and 15 m is assumed in our elevation measurements for the three terraces assigned to MIS 5e, 7, and 9, respectively (see below and Table 2). We thus incorporate these uncertainties in our elevation estimates of shoreline angles and derived uplift rates.

[27] The marine terraces at Arauco are cut into various types of bedrock (Figure 2b) and generally consist of shallow marine sediments overlain by a veneer of fluvial conglomerates (up to 3 m thick) and locally by eolian sands. The best developed and widest terrace in the Arauco region is the Cañete surface, which was identified and correlated with MIS 5e by Kaizuka et al. [1973] on the basis of its width, lateral continuity, and degree of preservation of stratigraphic features. In 2004, we sampled quartz pebbles from fluvial conglomerates overlying marine deposits of the Cañete Formation, and underlying the abandoned Cañete surface (Figure 3b) for exposure dating using ^{10}Be and ^{26}Al in situ produced cosmogenic nuclides (Table 1, see auxiliary material for a detailed explanation of the dating methods). These ages define terrace abandonment as fluvial incision occurred because of base level lowering, likely caused by the sudden drop in sea level at the end of an

interglacial or interstadial period combined with tectonic uplift [e.g., *Chappell and Shackleton*, 1986]. We restricted our sample locations to pristine, in situ terrace surfaces, an assessment that is further corroborated by the lack of of bioturbation within the underlying gravels and that original depositional imbrication is still intact. We were not able to collect surface samples as the surfaces did not contain any quartz pebbles. However, we were able to collect four subsurface samples at three sites that approximate the age of the Cañete terrace very well. We found the best sampling sites to be vertical road cuts that we enlarged and where both the marine and fluvial units were exposed. In some cases the underlying bedrock was exposed as well. A representative outcrop of the fluvial gravels sampled for cosmogenic dating can be found on Figure 3b.

[28] Our limited, but precise ages from the Cañete surface corroborate the inference of *Kaizuka et al.* [1973] that this surface was formed during the last interglacial. Following the same principles of *Kaizuka et al.* [1973], we tentatively assign the two upper surfaces (Esperanza and Nochas surfaces) to MIS 7 and 9, respectively. Similar geomorphic characteristics identify these surfaces as abrasion platforms that were sculpted during two separated, protracted sea level highstands that preceded the last interglacial highstand. As shown in section 4.3.1, uplift and shortening rates obtained with these assumptions agree very well within uncertainties with rates calculated from the isotopically dated Cañete surface.

4. Results: Deformation, Uplift, and Exhumation of the Nahuelbuta Range and Arauco Peninsula

[29] In order to characterize the Pliocene to recent tectonic history and its relation to the structural style of the Arauco-Nahuelbuta region, to quantify surface uplift rates, and to explore their along-strike variability and relation to active faults, we have studied deformation markers in the coastal realm at various timescales. We describe these deformation markers chronologically: Early Pliocene exhumation patterns based on fission track ages, late Pliocene and Pleistocene growth strata, regionally deformed Pleistocene marine terraces, and clusters of crustal seismicity and their relation to active faults mapped from seismic reflection profiles and field observations.

4.1. Thermochronology of the Nahuelbuta Range

[30] Fission track (FT) cooling ages from the Nahuelbuta Range have been reported by *Glodny et al.* [2008b]. In order to explore the spatial patterns of these ages in terms of the local structures, we projected their positions along a profile normal to the neotectonic warping axis of the Nahuelbuta Range and the Arauco peninsula and plotted them together with a topographic swath profile of a 50×150 km region (Figure 4c). The zircon FT ages display a rather flat pattern along the entire profile with no relation to the topography. Conversely, the apatite FT data describe a curved pattern that follows the domal topography of the Nahuelbuta Range and the Arauco peninsula anticline. In an age-elevation plot (Figure 4d), the apatite FT data continuously decrease in age with increasing elevations, which is opposite to that observed in most actively uplifting mountain ranges of the world [e.g., *Fitzgerald et al.*, 1993]. This indicates that

higher magnitudes of exhumation have been taking place in the more elevated parts of the range.

[31] At Nahuelbuta, the positive correlation between exhumation and topography, the inverse apatite FT age-elevation relation, and the early Pliocene increase in cooling/exhumation rate indicates that this sector of the Coastal Cordillera has been anomalous in terms of exhumation and probably rock uplift rate since early Pliocene time.

4.2. Deformation and Sedimentary Patterns of the Tubul Formation

[32] The Tubul Formation consists of sandstone and minor siltstone deposited in a shallow water, nearshore shelf environment during late Pliocene to early Pleistocene time [*Nielsen and Valdovinos*, 2008]. Deposits of the Tubul Formation overlie the earlier units with a marked angular unconformity [e.g., *Biró*, 1979; *Brüggen*, 1950; *Pineda*, 1986]. The Cañete Formation at the Arauco peninsula rests unconformably on the upper section of this unit (see below).

[33] Outcrops of the Tubul Formation are restricted to the northern and southern sectors of the Arauco peninsula on the flanks of Cretaceous to Eocene strata (Figure 2b). The thickness of the Tubul Formation increases away from the center of the peninsula; both toward the north and south, as constrained by 15 boreholes and the overall distribution of outcrops (Figure 6a). In the northern sector, near the town of Tubul, the lowermost exposures on vertical sea cliffs (analogous to Figure 3a) strike east-west and dip ~4 to 6° north; the dip decreases gradually up sequence to subhorizontal near its top, which in this region is covered by the subhorizontal marine and fluvial sediments of the Cañete Formation (Figure 3a). These field geometries are consistent with the seismically imaged syncontractional growth strata in the Arauco Bay, immediately to the north (Figure 2b) [*Melnick et al.*, 2006a], and the southward-thinning wedge geometry along the northern flank of the peninsula. The situation is similar in the southern sector of the peninsula, but there the lowermost exposed levels dip and increase in thickness to the south (Figure 6a). Growth strata of the Tubul Formation in sea-cliff exposures farther south in the Coi-Coi region at 38.5°S are also compatible with syncontractional deformation [see *Melnick and Echtler*, 2006a, Figure 3].

[34] Reflection seismic profile ENAP 28 is oriented north-south and located immediately south of the peninsula (Figure 7, profile location shown in Figure 2b). The ENAP exploration borehole "D," situated above profile 28 farther south, encountered the continental basement below 624 m of Tubul sediments. This unconformity is clearly imaged in many seismic lines of the fore-arc basins in south-central Chile [*González*, 1990; *Melnick and Echtler*, 2006a]. Profile 28 images two northwest striking, high-angle reverse faults responsible for the syncontractional deposition of the Tubul Formation. Both faults are blind and propagate anticlines. This profile images a lower unit characterized by low-amplitude, discontinuous and parallel reflectors, and an upper unit formed by higher-amplitude, continuous reflectors. Reflectors in the upper unit decrease in dip up sequence and exhibit internal onlapping and changes in thickness. Both units are deformed by an anticline, which is propagated by a blind reverse fault that only cuts and offsets the lower unit. An asymmetric hinge graben is imaged
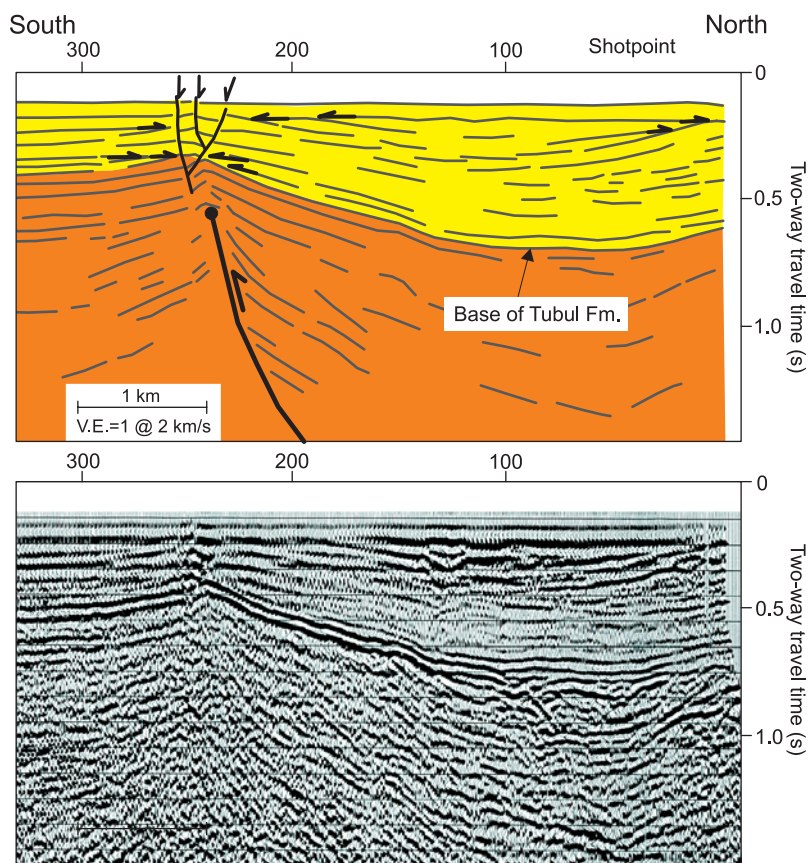
Figure 7. Example of an offshore seismic reflection profile showing a representative high-angle reverse fault and syncontractional fabrics of the Tubul Formation. Image extracted from profile ENAP 28. Location shown in Figure 2b. See detailed description in text.

above the tip of the anticline controlling the northward tilt of a central block. On the basis of the internal seismic fabrics, i.e., reflector continuity and thickness variability, we interpret the lower unit as precontractional and the upper one as syncontractional. Correlation with borehole D indicates that the upper unit corresponds to the Tubul Formation. Deposition of Tubul strata was coeval with contractional deformation and growing of the reverse fault cored anticline.

[35] Taken together, these field, borehole, and seismic data suggest that deposition of the Tubul Formation on the Arauco peninsula was associated with a major west-north-west trending growing anticline (Figure 8). This is in line with several offshore reverse fault-cored growth anticlines, which resulted from the inversion of Miocene to early Pliocene normal faults [*Melnick and Echtler*, 2006a].

4.3. Deformation and Sedimentary Patterns of Pleistocene Marine Terraces

[36] These three marine terrace surfaces were first described by *Kaizuka et al.* [1973]. These surfaces are abrasion platforms carved into bedrock and are covered by a veneer of sediments that record a finite moment of uplift and abandonment. The best expressed and preserved is the Cañete surface (Figures 3, 4, and 6). We refer to the sedimentary deposits that underlie the Cañete surface as the Cañete Formation. In the northern and southwestern sectors

of the peninsula the Cañete Formation overlies the Tubul Formation whereas in the central and southeastern parts it covers the Cretaceous and Eocene units (Figure 2b). The sediments of the Cañete Formation consist of two units: (1) a lower unit dominated by black, volcanic-derived sandstone with coarse cross bedding, flaser bedding, float tuffs, and occasionally interbedded layers of siltstone that contain charcoal, root casts, and fossil leaves and (2) an upper unit formed by well-rounded conglomeratic gravel and lenses of sandstone, which in the southern sector locally contain marine fossils. Locally, the upper unit is covered by homogenous, well-sorted medium sandstone with insect burrows and fine lamination, and paleosol horizons. This unit is clearly associated with elongated narrow ridges, which are topographically higher than the Cañete surface. We interpret the lower unit of the Cañete Formation as having been deposited in a coastal environment in the immediate vicinity of sea level; the upper unit as being related to a braided river system in transition from continental to deltaic environments. Fluvial sediments of this unit yielded mean ^{10}Be-^{26}Al pooled ages ranging from 127 ± 13 to 133 ± 14 ka (see methods for details; sample location in Figures 3b, 3d, and 4a). The areally restricted unit is interpreted as having been deposited in a coastal dune environment governed by southwesterly winds, similar to present conditions. This unit might have been deposited immediately after abandonment of the Cañete surface.
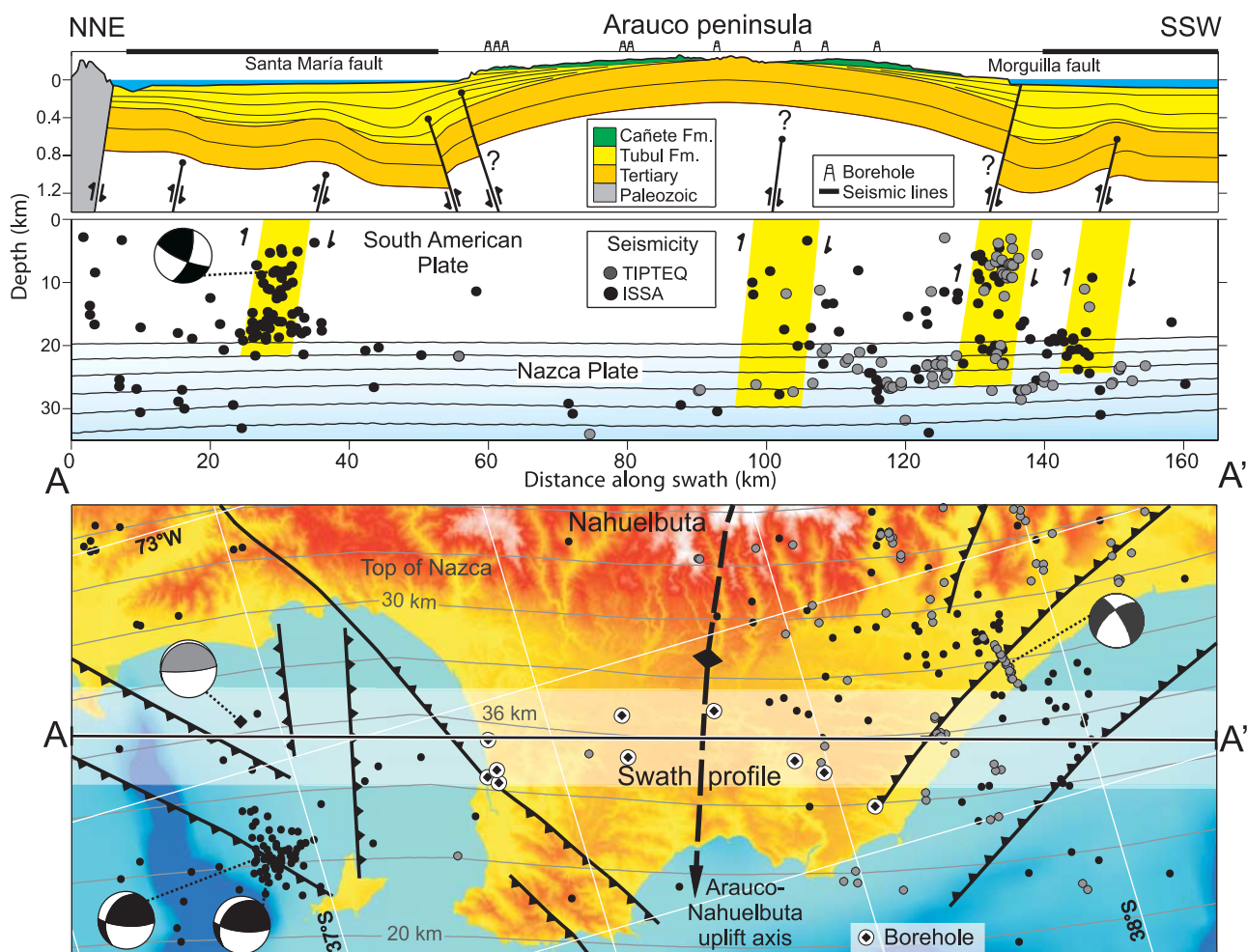
Figure 8. Profile of surface and crustal structure along the Arauco peninsula. Surface profile with maximum topography along swath shown by shaded rectangle in the center of the map. Fault dips are only apparent because of vertical exaggeration. Seismicity and focal mechanisms of the ISSA [*Bohm*, 2004; *Bohm et al.*, 2002; *Bruhn*, 2003] and TIPTEQ [*Haberland et al.*, 2006] local networks. Depth of the Tubul and Cañete formations from ENAP boreholes and exposed sections in the field (see Figure 6). Contours in the blue region labeled Nazca plate represent the top of the slab projected from 10 km spaced, parallel lines in the area of the map (2 km contours also shown in the map). Slab geometry from *Tassara et al.* [2006]. Shallow structures from the northern sector integrated from seismic reflection profiles described by *Melnick et al.* [2006a]; southern sector from profile ENAP 28 (Figure 7). Gray focal mechanism from U.S. Geological Survey National Earthquake Information Center catalog (21 May 1990, M_w 6.3, 5 km depth).

[37] The thickness of the Cañete Formation underlying the Cañete surface increases from a minimum of 20 m in the center of the peninsula to a maximum of at least 50 m in the southern and northern sectors (Figure 6b). Similarly, the elevation of the shoreline angle of the Cañete surface increases toward the center of the peninsula, where it reaches a maximum of 231 m (Figure 4b). These opposed variations in thickness and shoreline elevation are consistent with deposition contemporaneous with growth of an anticline, whose axis is oriented westnorthwest to east-southeast.

[38] The Esperanza and Nochas surfaces are exposed in the central part of the peninsula and the western flank of Nahuelbuta (Figure 4b). They are less well preserved than the Cañete surface, but still contain marine and fluvial deposits with clear treads and paleocliffs (Figures 3c and 6c). The position of their shoreline angle reaches maximum elevations of 360 and 471 m, respectively, mimicking the pattern of the Cañete surface in the center of the peninsula. Because of a regular elevation spacing between these three surfaces and similar distribution of their shoreline angles (Figure 4b), we infer that the Esperanza and Nochas surfaces were formed associated with sea level highstands at MIS 7 and 9, which preceded the last interglacial highstand responsible for the formation of the Cañete surface. Although correlating MIS 7 and 9 to the two upper surfaces is tenuous, the age-elevation relationships in conjunction with the isotopically dated Cañete surface yields very similar uplift and shortening rates (see subsections below and Table 2).
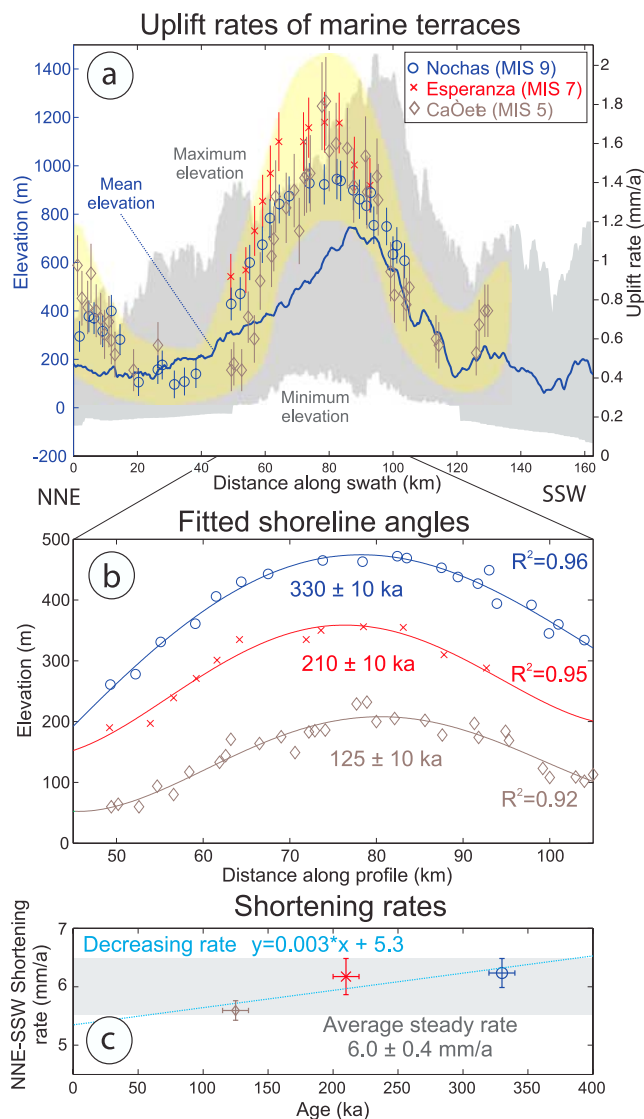
Figure 9. Uplift and shortening rates. (a) Surface uplift rates for the Cañete, Esperanza, and Nochas terrace surfaces of the Arauco peninsula and topographic swath profile (same as in Figure 4). Note that uplift rates of the three surfaces agree well within errors (yellow band). (b) Elevation of shoreline angles from the anticline in the center of the Arauco peninsula and fitted polynomial curves. (c) Shortening rates for the three marine surfaces estimated using line length balancing of the curves in Figure 9b. Given the uncertainties, shortening rate has either slowly decreased or remained constant.

4.3.1. Uplift, Deformation, and Tilt Rates Deduced From Marine Terraces

[39] We estimate surface uplift rates for 96 elevation measurements of shoreline angles from the Cañete, Esperanza, and Nochas Pleistocene surfaces (Figure 4b). Ages, paleo sea-level elevations, and the respective uncertainties of each marine oxygen isotope stage are presented in Table 2; uplift rates are shown in Figure 9a. In the center of the peninsula, where the three surfaces are well pre-

served, their uplift rates agree within errors. Uplift rates peak in the core of the peninsula reaching 1.8 ± 0.2 mm/a, and decrease toward both ends in the north and south to a minimum rate of 0.36 ± 0.07 mm/a (Figure 9a). These uplift rate gradients are likely caused by warping about the WNW−ESE oriented anticline whose axis is in the center of the peninsula (Figures 4a and 4b).

[40] Uplift rates north of the Arauco peninsula increase suddenly from $0.4−0.5$ to $0.7−0.9$ mm/a (between distance 0 and 20 km in Figure 9a). This increase is coincident with a slight rise in mean topography, with the position of the Coronel promontory (Figures 4a and 4b), as well as with a WNW−ESE striking and NNE dipping reverse fault mapped from offshore seismic profiles (Figure 2b). Thus, it is likely that this fault extends onshore and that it has been responsible for the gradient in uplift rates and coastline morphology. The vertical slip on this fault would be about $0.3−0.5$ mm/a.

[41] Along the southern coast of Arauco the Morguilla fault line scarp offsets the Cañete surface. The height of this scarp is 150 m at its northwestern edges and diminishes to ∼40 m toward the southeast near Lake Lanalhue where it is covered by active dunes (Figure 3d). Considering the MIS 5e age of the Cañete surface yields variable slip rates of $1.2−0.3$ mm/a. These rates should be considered as minimum because of the recent deposition of eolian sediments along the scarp.

[42] The Cañete surface is slightly tilted to the east. However, this eastward tilt is only clearly visible in the central, highest and widest part of the surface as illustrated in the WNW−ESE oriented swath profile in Figure 6c. The eastward tilt rate along this profile is $0.001−0.002°$/ka. Tilt rates of the northern and southern flanks of the anticline depicted in the NNE−SSW oriented swath profile in Figure 6c are on the same order of magnitude, reflecting a long-wavelength feature related to the open fold depicted in Figure 8.

[43] The maximum uplift rate obtained at the Arauco peninsula is similar to the uplift rate at Isla Santa María of 1.8 ± 0.4 mm/a over the past ∼50 ka [*Melnick et al.*, 2006a] and of 2.3 ± 0.2 mm/a over the past ∼3 ka [*Bookhagen et al.*, 2006]. However, the respective tilt rates of ∼0.025 and $0.022°$/ka determined for both timescales at Isla Santa María are significantly higher than the subdue rates of $0.001−0.002°$/ka estimated at Arauco. High tilt rates at Isla Santa María have likely been caused by slip on a blind thrust below the island that propagates a tight anticline, whereas the lower tilt rate at Arauco is apparently caused by the open fold that forms the peninsula.

4.3.2. Shortening and Strain Rates of the Arauco Peninsula Anticline

[44] Information gathered from seismic reflection profiles and thickness distribution of the Tubul and Cañete formations suggests that most of the contractional strain that accumulated during deposition of these two units over the past ∼2.5 Ma was oriented NNE−SSW. In order to estimate the amount of shortening responsible for folding and uplift of the Arauco peninsula anticline we use the shoreline angles of the Cañete, Esperanza, and Nochas marine surfaces. The erosional and depositional nature of these surfaces implies deposition on a seaward-dipping bedrock surface with a gentle slope of less than ∼0.1° [e.g., *Lajoie*, 1986],

which can be considered subhorizontal along strike to estimate shortening rates. We use the line length balancing technique to estimate shortening magnitudes and rates [e.g., *Ramsay and Huber*, 1987]. Plane strain is assumed, which may not be fully the case given that the Cañete surface is slightly tilted to the east (Figure 6c) and that plate convergence is oblique to our cross section (see discussion). In any case, our surface and borehole data suggest that the majority of the syntectonic growth of the Tubul and Cañete formations was a result of NNE−SSW oriented shortening over at the past ~2.5 Ma (Figures 6a and 8).

[45] In order to estimate line length changes, we fitted polynomial functions to the shoreline angle elevation measurements of each marine surface and projected them along a NNE−SSW profile (Figure 9b). The interpolated along-strike lengths of the folded shorelines were then compared to the horizontal distances to calculate amounts of finite shortening. Shortening was estimated only for the major, 60 km wide fold in the center of the peninsula, where the terraces are best expressed, and which is aligned with the topographic axis of the adjacent Nahuelbuta Range and area of enhanced exhumation. Shortening magnitudes and rates are shown in Table 2 for each surface. Shortening rates for the Cañete, Esperanza, and Nochas terraces are 5.6 ± 0.2, 6.2 ± 0.3, and 6.2 ± 0.2 mm/a, at a strain rate of -2.9, -3.1, and -3.2×10^{-16} s^{-1}, respectively. Average shortening is 6.0 ± 0.4 mm/a; rates decrease linearly within uncertainties at an average of 0.3 mm/a/10^5 a (Figure 9c).

4.4. Active Crustal Faults From Shallow Seismicity and Seismic Reflection Profiles

[46] The temporary Integrated Seismological Experiment in the Southern Andes (ISSA) and TIPTEQ amphibious local seismic networks deployed 62 and 70 broadband land seismic stations and several OBS/OBH in the Arauco region during 2000 and 2004–2005, respectively [*Bohm*, 2004; *Bohm et al.*, 2002; *Bruhn*, 2003; *Haberland et al.*, 2006]. These data demonstrate that most of the seismicity in the upper plate is concentrated in the fore-arc region below the shelf and coast. Shallow earthquakes ($\leq M$ 5) cluster in two regions surrounding the Arauco peninsula (Figure 8). In a previous study, we have shown that the northern cluster adjacent to Isla Santa María is related to a steep northeast-striking reverse fault, which is apparently rooted in the plate interface [*Melnick et al.*, 2006a]. The southern cluster is located below the steep, up to 150 m high northwest-striking Morguilla fault scarp (Figures 3d and 8). Analogous to the region surrounding Isla Santa María, earthquakes associated with the Morguilla fault form a cluster with a continuous alignment in cross section from a depth of 5 km until the plate interface, which below this region is at about 27 km depth (Figure 8). Shallow focal mechanisms are compatible with a northwest-striking, northeast-dipping reverse fault with minor strike-slip components [*Bruhn*, 2003; *Haberland et al.*, 2006].

[47] Similar to the Isla Santa María and Arauco Bay areas, seismic reflection data immediately south of the Morguilla fault image steep reverse faults that control the syncontractional deposition of the late Pliocene to Quaternary units (Figures 2b and 7). We thus consider it likely that the Morguilla scarp is the surface expression of a deep-reaching, northwest-striking reverse fault that dips steeply to the northeast. However, this scarp might have been modified by recent coastal erosion and eolian deposition.

5. Discussion
5.1. Deformation, Surface Uplift, and Exhumation of the Nahuelbuta Range and Arauco Peninsula

[48] Our integrated stratigraphic and structural data from the Arauco region suggests that margin-parallel, continuous shortening starting in the early Pliocene has led to the emergence of the continental shelf and topographic development of the Nahuelbuta Range and Arauco peninsula. Apatite fission track data shows that exhumation in the central part of Nahuelbuta records an order of magnitude increase at a central age of 4 Ma, from 0.03 mm/a to greater than 0.2 mm/a [*Glodny et al.*, 2008b]. Despite modeling uncertainties of 30%, this age agrees well with related tectonic events with independent age constraints, such as the onset of inversion of the extensional Arauco fore-arc basin [*Melnick and Echtler*, 2006a] and collision of the Chile Rise [*Cande and Leslie*, 1986]. The collision of the Chile Rise has led in turn to accelerated exhumation and strike-slip motion of the Liquiñe-Ofqui fault zone (see below). The correlation between the dome-like morphology of the Nahuelbuta Range and the warped distribution of fission track ages with higher amounts of exhumation in the central, higher-elevation parts of the range (Figure 4), suggests that tectonic growth by asymmetric doming has controlled local exhumation in an area of ~1200 km^2. In contrast, adjacent sectors of the Coastal Cordillera near Concepción (36.5°S) and Valdivia (40°S) have remained relatively stable and have been exhuming at a low steady rate of 0.03–0.04 mm/a since Triassic time [*Glodny et al.*, 2008b].

[49] The thickness of the late Pliocene to early Pleistocene Tubul and of the ~125 ka old Cañete formations increases away from the WNW−ESE oriented main warping axis toward the edges of the peninsula (Figures 6, 7, and 8). The three marine terrace surfaces along the western, coastal flank of Nahuelbuta and along the Arauco peninsula have been folding about this same axis at a shortening rate of ~6 mm/a over the past ~330 ka, resulting in coeval uplift at a variable rate between 0.3 and 1.8 mm/a across the strike of the anticline (Figure 9). We interpret these changes in thicknesses to reflect deposition coeval to growth of the Arauco anticline accommodating margin-parallel shortening.

[50] Marine seismic reflection profiles off the northern and southern edges of the Arauco peninsula image blind high-angle reverse faults at the core of fault propagation anticlines (Figures 2b, 7, and 8). Some of these faults occur in the immediate vicinity of crustal seismicity clusters ($\leq M$ 5.2). The alignment of seismicity is compatible with the steep fault dip angles predicted by focal mechanisms, suggesting that microearthquakes illuminate crustal-scale faults, some of which appear to be rooted in the plate interface thrust (Figure 8). The spatial coincidence between the distribution of topography, exhumation gradients, uplifted and warped marine terraces, Pliocene and Pleistocene growth strata (Figures 4 and 6), and active reverse faults suggests that uplift of the Arauco peninsula is controlled by these deep-reaching structures (Figure 8).

One of these structures is the Morguilla fault, which appears to be associated with the Lanalhue fault zone (Figures 2b and 3c), a margin-scale, seismically active fault system inherited from Paleozoic time [*Glodny et al.*, 2008a] (Figure 8). These observations emphasize the role of inherited upper plate fabrics in guiding and focusing active plate boundary deformation in this environment.

5.2. Uplift and Deformation Mechanisms of the Arauco-Nahuelbuta Fore-Arc Block

[51] The Arauco peninsula and Nahuelbuta Range are part of an anomalous segment of the Chilean margin in terms of topography, geology and exhumation. The former is a major anomaly of the coastline along the Pacific shore of South America, where the trench-to-coast distance reaches a local minimum, whereas the latter coincides with an area where the mean elevation of the Coastal Cordillera is double the average typical of south-central Chile. Interestingly, this correlates spatially with focused Pliocene-Recent exhumation at Nahuelbuta and maximum uplift rates determined from Pleistocene marine terraces at the center of Arauco reaching 1.8 ± 0.2 mm/a, which is nearly twice the average rate of 0.9 ± 0.4 mm/a between 33.5 and 40°S (based on data compiled by *Melnick and Echtler* [2006a]). These high rates are interpreted in terms of focused shortening and uplift. We further explore the tectonic processes responsible for this focused deformation in terms of lower and upper plate features.

5.2.1. Role of Lower Plate Anomalies and Trench Sediments

[52] Previous studies have proposed that the Mocha Fracture Zone, which today is subducted underneath Arauco (Figure 1b), is responsible for the anomalous rapid emergence of the peninsula during the Quaternary [*Boettcher*, 1999; *Kaizuka et al.*, 1973; *Lohrmann et al.*, 2006]. However, our integrated data suggests ongoing uplift and folding of the Arauco-Nahuelbuta region since ~4 Ma, when the intersection of the Mocha Fracture Zone with the margin occurred ~400 km north. Thus, the Mocha Fracture seems unlikely to be responsible for the pronounced and protracted localized uplift of the Arauco peninsula and Nahuelbuta Range.

[53] Another process that could explain the anomalous uplift of the Arauco-Nahuelbuta region would be localized underplating and basal accretion of subducted trench sediments. In fact, south of 33°S, the Chile trench has been filled with over 1 km of sediments since Pliocene time [*Bangs and Cande*, 1997]. Basal accretion has been suggested as a major process in Paleozoic accretionary tectonics of this region [*Glodny et al.*, 2005], but its imprint on Cenozoic tectonics has not been yet observed in geophysical images [e.g., *Krawczyk et al.*, 2006; *Ranero et al.*, 2006]. Sediments in the Chile trench are mostly supplied by rivers that drain the high Andes cutting across the Coastal Cordillera, and are deposited in large submarine fans [e.g., *Thornburg et al.*, 1990]. Transport of sediments northward along an axial channel in the trench seems to be related to glaciations and have occurred only during the Holocene [*Völker et al.*, 2006]. Thus, the size of the fans in this system largely determines the amount of sediments available for frontal and basal accretion. If basal accretion would be indeed occurring, it should be more pronounced inland of the large fans, where trench fill is thicker [*Völker et al.*, 2006]. Large fans have been imaged off the mouth of every major river in south Chile [*Thornburg et al.*, 1990]; however, no clear relation between their positions and localized coastal uplift is apparent [*Rehak et al.*, 2008]. The largest fan in this region is the Bío-Bío fan, located 50 km north of Arauco (Figure 2b). Thus, underplating and basal accretion of trench sediment as well as increased deformation and uplift of the upper plate would be expected to occur landward of the Bío-Bío river mouth, in vicinity of Concepción (Figures 2a and 2b). However, this region has experienced slower exhumation and uplift than at Arauco (Figure 9a) resulting in a subdued topography. Hence, underplating and basal accretion of trench sediments are probably not viable processes to explain localized uplift, exhumation, and margin-parallel shortening observed in the Arauco-Nahuelbuta region.

5.2.2. Role of the Segmented Upper Plate

[54] The Arauco peninsula is in the northern sector of the Chiloé block, a fore-arc sliver decoupled from stable South America by the dextral Liquiñe-Ofqui fault zone (LOFZ) [e.g., *Cembrano et al.*, 2002; *Hervé*, 1994]. Dextral shear along the LOFZ increased at ~6 Ma triggered by an augment in convergence obliquity and by collision of three consecutive segments of the Chile Rise at the trailing edge of the Chiloé block, located near the Taitao peninsula at 46.5°S (Figures 1a and 10) [e.g., *Cande and Leslie*, 1986; *Cembrano et al.*, 2002; *Rosenau et al.*, 2006; *Thomson*, 2002]. Thus, a synchronous acceleration is expected in the northward motion of the fore-arc sliver. The mean slip rate along the LOFZ over the past ~6 Ma decreases from ~32 to ~13 mm/a northward along the Chiloé block [*Rosenau et al.*, 2006], consistent with high partitioning of oblique convergence. Similarly, GPS data show the highest margin-parallel rates of ~6 mm/a in the southern sector of the Chiloé block and a continuous decreases northward [*Wang et al.*, 2007]. Unfortunately, no slip rate data of the LOFZ exist yet on intermediate time scales ($10^5 – 10^3$ years).

[55] Our regional inspection of marine terraces south of Arauco revealed deformation along discrete reverse faults with strike-slip components that are oriented oblique to the margin, like the Mocha-Villarica fault (Figure 2b). This supports the hypothesis that part of the margin-parallel component of oblique plate convergence is absorbed internally within the sliver, as originally suggested by *Rosenau et al.* [2006]. However, these structures are high-angle reverse faults that propagate open folds and control long-wavelength tilting, which does not account for much shortening. Our integrated data shows that ~6 mm/a of margin-parallel shortening have been accommodated at Arauco over the past 330 ka, and that this shortening has been active since ~4 Ma. This rate is slower than the ~13 mm/a stike-slip rate predicted for the northern LOFZ by *Rosenau et al.* [2006], and therefore suggests either a substantial decrease in sliver motion, as may be expected from the documented decline in plate convergence rate, or partial accommodation of sliver motion elsewhere.

[56] Major changes in fault kinematics and structural style occur at the latitude of Arauco-Nahuelbuta along the intra-arc and foreland regions to the east. For example, the LOFZ ends at the Callaqui-Copahue-Mandolegüe volcanic lineament (38°S), which marks a major transition along the
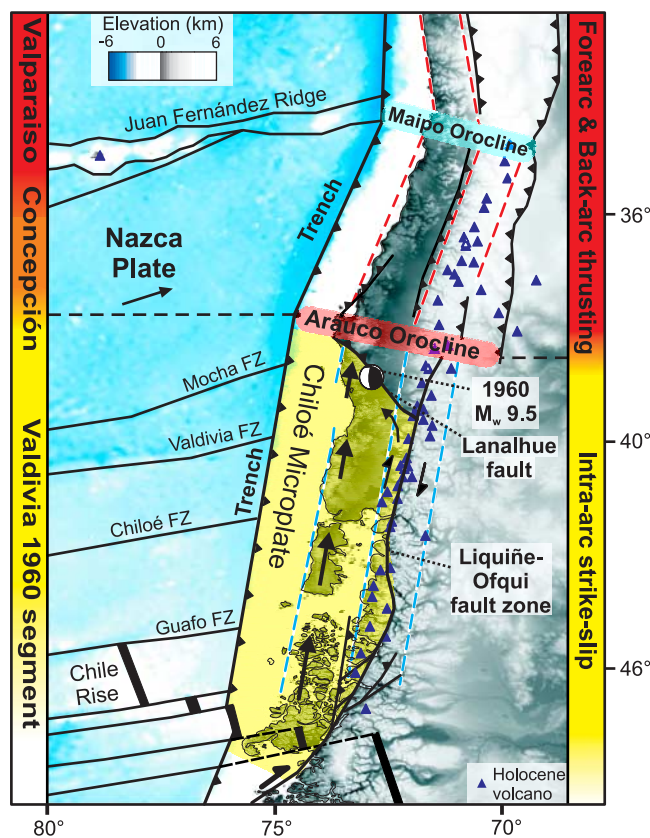
Figure 10. Seismotectonic model. Oblique plate convergence and subduction of the Chile Rise leads to decoupling of the Chiloé fore-arc sliver along the Liquiñe-Ofqui fault zone. Margin-parallel northward motion is partly accommodated internally along the sliver and by NNE−SSW shortening in the Arauco region, resulting in doming of the Nahuelbuta ranges and emergence of the Arauco peninsula. As a result of this collision, the entire orogen bends eastward at the Arauco Orocline, which also marks a boundary between deformation styles in the intra-arc and foreland regions. The coincidence between the extent of the Valdivia 1960 rupture segment and the Chiloé fore-arc sliver suggests that here the fore-arc structure controls the extent of megathrust rupture segments.

high Andes in terms of kinematics and structural styles [*Folguera et al.*, 2002; *Melnick et al.*, 2006b]. Importantly, to the north of this boundary, east-directed thrusting occurs continuously along the eastern foothills and foreland of the Andes for over 5000 km along strike. In contrast, to the south of this boundary active deformation is limited to the intra-arc, while the back arc has remained tectonically inactive since the latest Miocene. These structural changes clearly reflect variations in the degree of strain partitioning of oblique subduction. Partitioning is high south of 38°S, where most of the margin-parallel component of oblique subduction is accommodated along the discrete strike-slip LOFZ (Figure 10). Conversely, to the north of 38°S margin-parallel strain is diffusely distributed across the entire active margin, reflecting a lower degree of partitioning [*Melnick et al.*, 2006b].

[57] In addition to these kinematic and structural gradients, the orientation of the Andean orogen including the trench, coastline, topographic axes of the Coastal Cordillera, western flank of the Main Cordillera, and the axis of the volcanic arc, bend about 10° to the east across the boundary at 38°S. We refer to this morphological, structural, and kinematic boundary as the Arauco Orocline (Figure 10). The axis of this orocline is oriented WNW−ESE, parallel to the Arauco-Nahuelbuta uplift axis and aligned with the position of the Callaqui-Copahue-Mandolegüe transition zone in the intra-arc region. This transition zone has decoupled the dextral LOFZ from back arc shortening since the Pliocene and is expressed by an 80 km long alignment of Pliocene-Quaternary volcanic centers [*Folguera et al.*, 2002], the largest alignment of the Southern Volcanic Zone. The data presented in this study from the fore-arc region and previously from the intra-arc [*Melnick et al.*, 2006b] suggests that this boundary has been active contemporaneously in both domains since Pliocene time.

[58] The Nazca plate below Nahuelbuta dips 12.7°, in contrast to 19.2° and 15° to the north and south, respectively [*Krawczyk et al.*, 2006] (Figure 8). A lower dip angle results in higher shear traction at the base of the continental plate, manifested in faster landward interseismic GPS velocities [*Moreno et al.*, 2008]. We suggest that oroclinal bending at Arauco is a response to a northward translation of the Chiloé fore-arc sliver and collision against a buttress, which results from the combined effect of a shallower slab dip and strength contrast between heterogeneous metamorphic rocks to the south and the homogeneous granites in the Nahuelbuta Range (Figure 2b). This buttress would be caused by a change in physical conditions following the model of [*Beck et al.*, 1993]. This strength contrast and difference in material properties south of Nahuelbuta is also suggested by a ∼40 mGal gradient of the Bouger gravity field [*Hackney et al.*, 2006] as well as a ∼20 km gradient in elastic thicknesses [*Tassara et al.*, 2007], and a reduction in P wave velocity of the crust determined from 3-D tomography [*Bohm*, 2004].

[59] The Andean margin is characterized by another bend in strike at 34°S, referred to as the Maipo Transition Zone [*Yáñez et al.*, 2002] or Maipo Orocline [*Farías et al.*, 2008], interpreted to result from collision of the Challenger Fracture Zone and Juan Fernández Ridge with the continent since 25 Ma [*Yáñez et al.*, 2002] (Figure 10). Late Cenozoic margin-parallel fore-arc shortening has also been documented in northern Chile and southern Perú [*Allmendinger et al.*, 2005a]. There, however, bending of the Bolivian Orocline over at least the past ∼30 Ma, and rotation of fore-arc blocks about vertical axes seems to account entirely for this shortening [*Allmendinger et al.*, 2005b].

[60] A good analog to the setting in south-central Chile is the Cascadia margin of the northwestern United States, where margin-parallel northward translation of fore-arc blocks has been broadly documented with paleomagnetic, structural, and GPS data [e.g., *McCaffrey et al.*, 2007; *Wells et al.*, 1998]. Translation there leads to collision of the Oregon block with the Canadian Coastal ranges buttress resulting in margin-parallel shortening in the Puget Sound region, where several active reverse faults akin to the structures at Arauco strike nearly normal to the trench [e.g., *Johnson et al.*, 2004]. Collision produces transpres-

sion resulting in uplift of the Olympic Mountains and peninsula [*Wells et al.*, 1998], a major topographic anomaly along the Cascadia margin. The Olympic Mountains have a dome-like morphology with maximum elevations that double the surrounding regions, analogous to the Nahuelbuta Range. Quaternary and geodetic deformation along the coast of the Olympic peninsula is dominated by the Kalaloch syncline, a broad, low-amplitude fold whose axis is oriented ENE–WSW, nearly orthogonal to the margin [*Thackray*, 1998]. The Kalaloch syncline apparently accommodates margin-parallel shortening resulting from translation of the Oregon block. The Olympic peninsula could be thus considered analogous to the Arauco peninsula-Nahuelbuta Range block, although in a more evolved stage and subjected to glaciations.

5.3. Upper Plate Control on Segmentation of Subduction Earthquakes: Boundary Between the Valdivia and Concepción Seismotectonic Domains

[61] The magnitude of a subduction earthquake is thought to be controlled by the length and width that its rupture may achieve along the strike of the megathrust and by finite fault slip [*Hanks and Kanamori*, 1979]. Bathymetric features of the lower plate, such as fracture zones or seamounts, frictional instabilities along the plate interface or petrophysical discontinuities of the fore-arc resulting in mechanical heterogeneities have been proposed to act as major barriers that could potentially stall earthquake rupture propagation, thus limiting the finite magnitude [e.g., *Aki*, 1979; *Collot et al.*, 2004; *Taylor et al.*, 1987].

[62] In the Arauco-Chiloé region, the lower plate is cut by several fracture zones. Plate roughness, however, is smoothed by 1.5–2.3 km of sediments filling the trench before entering the interplate zone. The fact that the 1960 rupture propagated for ~1000 km across four of these fracture zones (Figure 1b) suggests that at least here lower plate anomalies have been unable to stall rupture propagation. Conversely, the 2001 Arequipa earthquake (M_w 8.4), which ruptured ~400 km of the Andean megathrust in southern Perú where the trench is virtually devoid of sediments, was stalled by a subducting fracture zone [*Robinson et al.*, 2006]. This fracture zone is similar in size to its counterparts in south-central Chile, suggesting that the amount of trench sediments may exert a major influence on smoothing lower plate bathymetric anomalies, and consequently limiting rupture propagation along the Andean megathrust. However, the Chile trench is continuously filled with over 1.5 km of sediments between 33 and 45°S, across the boundary between the Valdivia and Concepción seismic segments (Figure 1b). Thus, in the Arauco region neither bathymetric anomalies of the lower plate nor variable trench fill thicknesses present viable parameters to have influenced the position of this earthquake rupture boundary. We therefore further discuss a third possibility, which includes the control of inherited fore-arc heterogeneity and structure.

[63] Uplift and doming of the Arauco-Nahuelbuta region is likely a result of crustal thickening due to collision of the northward-translating Chiloé microplate; this crustal thickening increases the normal stresses on the megathrust and consequently the degree of interplate coupling. The shear stress necessary to rupture the megathrust is a function of plate convergence, the strength of the fault, and the normal stress or load of the fore-arc [e.g., *Scholz*, 2002]. Thus, a higher load generated by a thicker section of crust in the fore-arc at Arauco-Nahuelbuta would require higher shear stresses for failure. This could inhibit dynamic rupture propagation, ultimately controlling the position of the seismotectonic boundary. However, the higher topography at Nahuelbuta is in part compensated by a shallower angle of the subducting slab [*Hackney et al.*, 2006], and thus crustal thickness remains relatively constant along Nahuelbuta.

[64] The pioneer theoretical earthquake barrier model of *Aki* [1979] classified the barriers where earthquakes can start and/or stop as inhomogeneous and geometrical. The strength gradient caused by the sharp lithological transition across the Lanalhue fault, which juxtaposes heterogeneous metamorphic rocks with homogeneous intrusives (Figure 2b) likely represents an inhomogeneous barrier in the sense of *Aki* [1979]. This discontinuity marks pronounced anomalies in gravity, crustal P wave velocities, and elastic thickness, suggesting major changes in the petrophysical properties of the crust. The nature of the Lanalhue fault [*Glodny et al.*, 2008a], its expression in a deep reflection profile [*Groß et al.*, 2008], and the distribution of microseismicity [*Haberland et al.*, 2006] strongly suggest that this structure as well as the adjacent geological units extend through the entire crust. Thus, it is plausible that this inhomogeneous barrier extends to the interplate seismogenic zone. Coincidently, several $M > 7$ earthquakes of the 1960 sequence including the M_w 9.5 main shock were nucleated along the plate interface in the region adjacent to the Lanalhue fault (Figure 2a), following the conceptual model of *Aki* [1979]. These observations suggest that the limit between the Concepción and Valdivia megathrust rupture segments as well as initiation and propagation of Valdivia-type ruptures are controlled by the geological structure of the fore-arc.

[65] An inhomogeneous barrier analogous to the situation at Arauco-Nahuelbuta seems to exist at the Nankai margin of SE Japan. The position of this barrier below the Kii peninsula has controlled nucleation and propagation of subduction earthquakes from two adjacent seismotectonic segments [*Kodaira et al.*, 2006]. This barrier is highlighted by pronounced anomalies in gravity and P wave velocities as well as by the morphology of the coastline. The nature of this barrier has been attributed to the position of an old intrusive complex in the continental basement [*Kodaira et al.*, 2006].

[66] In this context we explore further regional tectonic features of the Chile margin and their effect on seismotectonic segmentation. The position of the Arauco peninsula is coincident with the northern termination of the Liquiñe-Ofqui fault zone, and the Valdivia earthquake rupture segment corresponds to the extent of the Chiloé fore-arc sliver (Figure 10). The basement of the entire Chiloé sliver south of Nahuelbuta consists of a rather homogenous unit of metamorphic rocks interpreted as a Paleozoic accretionary wedge [*Glodny et al.*, 2005]. The trench in this area is continuously filled with over 1.5 km of sediments along the sliver [*Bangs and Cande*, 1997]. Thus, both the upper plate and the plate interface along the entire Chiloé sliver are mechanically homogenous and decoupled from the continent; such homogeneity is thought to smooth the seismic

strength [*Ruff*, 1989], and therefore to facilitate dynamic propagation the earthquake rupture. We suggest that these factors controlled the giant magnitude of the 1960 earthquake, when rupture propagated for ∼1000 km along the entire length of the Chiloé sliver resulting in a M_w 9.5 event. At the Arauco peninsula, where historical ruptures of the Concepción and Valdivia segments have stopped, the basement character of the upper plate changes dramatically because of the appearance of intrusive rocks. The southern limit of the Valdivia segment corresponds to the southern Chiloé sliver, where the Chile Rise collides against the margin (Figure 1b), a geometrical barrier [*Aki*, 1979] whose high heat flow may contribute to inhibiting strong plate coupling and consequently earthquake rupture [e.g., *Hyndman and Wang*, 1995].

[67] Taking our observations together, we suggest that the Chiloé sliver and Arauco-Nahuelbuta block control the spatial extent of the Valdivia seismic segment. As our integrated study has demonstrated, collision of the Chiloé sliver has led to ongoing shortening at its northern, leading edge resulting in uplift of the Arauco-Nahuelbuta block over the past ∼4 Ma. During this time, the trench has been constantly filled with sediments derived from repeated Patagonian glaciations and two segments of the Chile Rise have impinged on the margin at the southern, trailing edge of the Chiloé sliver (Figure 10). Thus, we consider it also plausible that the extent and location of the Valdivia seismic segment, including its northern and southern boundaries at Arauco and Taitao peninsulas, respectively, has remained stable in space over the past few million years. Consequently, for this sector of the Andean margin, upper plate structural and petrophysical characteristics apparently play a major role in governing the segmentation of subduction earthquake ruptures.

6. Conclusions

[68] We have integrated a multidisciplinary data set to explore the kinematics of coastal deformation at various timescales in the Arauco-Nahuelbuta fore-arc sector of the south-central Chile margin. This sector corresponds to the overlapping boundary of two adjacent megathrust earthquake rupture zones, defined from ∼500 years of historical records. Here, similarities between topography, exhumation patterns derived from fission track dating, the spatial distribution of syntectonic sediments, and the character of uplifted and deformed marine terraces suggest that constant deformation mechanisms have led to sustained kinematics since the early Pliocene. Deformation has been dominated by margin-parallel shortening leading to localized uplift of the Arauco-Nahuelbuta block, whereas adjacent sectors of south-central Chile's Coastal Cordillera have remained stable. We interpret this localized margin-parallel shortening as a result of northward translation of the Chiloé microplate and of its collision against a buttress. This buttress may result from the conspiring effects of a sharp lithological transition in Paleozoic basement rocks and a shallower slab below the Arauco-Nahuelbuta block. The Chiloé microplate is a fore-arc sliver decoupled from stable South America by the arc-parallel Liquiñe-Ofqui strike-slip fault zone. Northward sliver translation parallel to the margin is a response to

oblique convergence between the Nazca and South American plates, as well as oblique collision and spreading of the Chile Rise at the sliver's southern trailing edge (Figure 10). Our interpretation of the conditions of the Arauco-Nahuelbuta fore-arc block is consistent with regional fault kinematic, thermochronologic, and geomorphic data that indicate decoupling of this fore-arc microplate and ongoing collision since early Pliocene time.

[69] The 1960 and 1835 subduction zone earthquake ruptures of the adjacent Concepción and Valdivia seismic segments taper off across the Arauco-Nahuelbuta block (Figure 2a), analogous to the estimated rupture zones of previous historical earthquakes (Figure 1b). The nucleation region of the 1960 sequence, which includes the M_w 9.5 main shock as well as several M_w > 7.9 fore and aftershocks, is located along the flank of the Arauco-Nahuelbuta block, adjacent to the Lanalhue fault (Figures 2a and 2b). This seismically active structure contains Paleozoic mylonites, juxtaposes two distinct units of the continental basement, and marks pronounced gradients in various geophysical data. We propose that the sharp gradient in petrophysical properties of the crust marked by the Lanalhue fault represents an inhomogeneous earthquake barrier, which controls initiation and propagation of Valdivia 1960-type megathrust ruptures.

[70] The extent of historical ruptures of the Valdivia segment equals the extent of the Chiloé microplate and of a segment of the Chile trench filled with over 1.5 km of sediments (Figure 10). These sediments derive from glacial erosion of the Patagonian Andes, a process that began during the Pliocene. We propose that mechanical homogeneity provided by a fore-arc microplate that is decoupled from the stable continent and by an interplate zone smoothed by trench sediments may facilitate rupture propagation for a distance in excess of 1000 km along the Valdivia segment, generating giant earthquake magnitudes such as during the 1960 event that reached M_w 9.5. We suggest that the boundary between the Valdivia and Concepción seismotectonic sectors and the extent of Valdivia-type earthquake ruptures have been sustained over the past few million years, because microplate decoupling resulting from oblique plate convergence and subduction of an active spreading center at its trailing edge, as well as collision causing uplift at its leading edge have been ongoing since the early Pliocene. These results emphasize the role of inherited upper plate fabrics in guiding active plate-boundary deformation and subduction zone earthquake segmentation processes.

References

Aki, K. (1979), Characterization of barriers on an earthquake fault, *J. Geophys. Res.*, *84*, 6140–6148, doi:10.1029/JB084iB11p06140.

Allmendinger, R. W., G. González, J. Yu, G. Hoke, and B. Isacks (2005a), Trench-parallel shortening in the northern Chilean fore-arc: Tectonic and climatic implications, *Geol. Soc. Am. Bull.*, *117*, 89–104, doi:10.1130/B25505.1.

Allmendinger, R. W., R. Smalley Jr., M. Bevis, H. Caprio, and B. Brooks (2005b), Bending the Bolivian orocline in real time, *Geology*, *33*, 905–908, doi:10.1130/G21779.1.

Alvarez, L. (1963), Studies made between Arauco and Valdivia with respect to the earthquakes of 21 and 22 May 1960, *Bull. Seismol. Soc. Am.*, *53*, 1315–1330.

Ando, M. (1975), Source mechanisms and tectonic significance of historical earthquakes along the Nankai trough, Japan, *Tectonophysics*, *27*, 119–140, doi:10.1016/0040-1951(75)90102-X.

Bangs, N. L., and S. C. Cande (1997), Episodic development of a convergent margin inferred from structures and processes along the southern Chile margin, *Tectonics*, *16*, 489–503, doi:10.1029/97TC00494.

Barrientos, S. (1987), Is the Pichilemu-Talcahuano (Chile) a seismic gap?, *Seismol. Res. Lett.*, *61*, 43–48.

Beck, M. E., Jr., C. Rojas, and J. Cembrano (1993), On the nature of buttressing in margin-parallel strike-slip fault systems, *Geology*, *21*, 755–758, doi:10.1130/0091-7613(1993)021<0755:OTNOBI>2.3.CO;2.

Beck, S., S. Barrientos, E. Kausel, and M. Reyes (1998), Source characteristics of historic earthquakes along the central Chile subduction zone, *J. South Am. Earth Sci.*, *11*, 115–129, doi:10.1016/S0895-9811(98)00005-4.

Beck, S. L., and L. J. Ruff (1989), Great earthquakes and subduction along the Peru trench, *Phys. Earth Planet. Inter.*, *57*, 199–224, doi:10.1016/0031-9201(89)90112-X.

Biró, L. (1979), Contribución al conocimiento de la Formación Tubul, Plioceno Superior, Provincia de Arauco (37°14′S), paper presented at 2nd Congreso Geológico Chileno, Serv. Nac. de Geol. y Minería, Arica, Chile.

Blumberg, S., et al. (2007), Coastal lakes in south-central Chile (38°S): Archives of Holocene climate and fore-arc tectonics, *EOS Trans. AGU*, *88*(52), Fall Meet. Suppl., Abstract PP31D-0653.

Boettcher, M. (1999), Tectonics of the Arauco peninsula and nearby fore-arc region (south-central Chile), *Mitt. Geol. 83*, pp. 1–58, Paläontologisches Inst. Univ. Hamburg, Hamburg, Germany.

Bohm, M. (2004), 3-D local earthquake tomography of the southern Andes between 36° and 40°S, Ph.D. thesis, 135 pp., Free Univ., Berlin.

Bohm, M., et al. (2002), The southern Andes between 36°S and 40°S latitude: Seismicity and average velocities, *Tectonophysics*, *356*, 275–289, doi:10.1016/S0040-1951(02)00399-2.

Bookhagen, B., H. P. Echtler, D. Melnick, M. R. Strecker, and J. Q. G. Spencer (2006), Using uplifted Holocene beach berms for paleoseismic analysis on the Santa María Island, south-central Chile, *Geophys. Res. Lett.*, *33*, L15302, doi:10.1029/2006GL026734.

Bourgois, J., et al. (2007), Tectonic record of strain buildup and abrupt coseismic stress release across the northwestern Peru coastal plain, shelf, and continental slope during the past 200 kyr, *J. Geophys. Res.*, *112*, B04104, doi:10.1029/2006JB004491.

Brüggen, J. (1950), *Fundamentos de la Geología de Chile*, 374 pp., Inst. Geogr. Mil., Santiago.

Bruhn, C. (2003), Momententensoren hochfrequenter ereignisse in sud Chile, Ph.D. thesis, 181 pp., Univ. of Potsdam, Potsdam, Germany.

Campos, J., et al. (2002), A seismological study of the 1835 seismic gap in south-central Chile, *Phys. Earth Planet. Inter.*, *132*, 177–195, doi:10.1016/S0031-9201(02)00051-1.

Cande, S. C., and R. B. Leslie (1986), Late Cenozoic tectonics of the southern Chile trench, *J. Geophys. Res.*, *91*, 471–496, doi:10.1029/JB091iB01p00471.

Cembrano, J., et al. (2002), Late Cenozoic transpressional ductile deformation north of the Nazca-South America-Antarctica triple junction, *Tectonophysics*, *354*, 289–314, doi:10.1016/S0040-1951(02)00388-8.

Chappell, J. M., and N. J. Shackleton (1986), Oxygen isotopes and sea level, *Nature*, *324*, 137–140, doi:10.1038/324137a0.

Cifuentes, I. L. (1989), The 1960 Chilean earthquakes, *J. Geophys. Res.*, *94*, 665–680, doi:10.1029/JB094iB01p00665.

Cisternas, M., et al. (2005), Predecessors of the giant 1960 Chile earthquake, *Nature*, *437*, 404–407, doi:10.1038/nature03943.

Collot, J. Y., et al. (2004), Are rupture zone limits of great subduction earthquakes controlled by upper plate structures? Evidence from multichannel seismic reflection data acquired across the northern Ecuador-southwest Colombia margin, *J. Geophys. Res.*, *109*, B11103, doi:10.1029/2004JB003060.

Comte, D., and M. Pardo (1991), Reappraisal of great historical earthquakes in the northern Chile and southern Peru seismic gaps, *Nat. Hazards*, *4*, 23–44, doi:10.1007/BF00126557.

Comte, D., et al. (1986), The 1985 central Chile earthquake: A repeat of previous earthquakes in the region?, *Science*, *233*, 449–453, doi:10.1126/science.233.4762.449.

Contreras-Reyes, E., I. Grevemeyer, R. Flueh, and C. Reichert (2008), Upper lithospheric structure of the subduction zone offshore of southern Arauco peninsula, Chile at ∼38°S, *J. Geophys. Res.*, *113*, B07303, doi:10.1029/2007JB005569.

Darwin, C. (1851), *Geological Observations of South America*, 279 pp., Smith and Elder, London.

Demets, C., R. G. Gordon, D. F. Argus, and S. Stein (1994), Effect of recent revisions to the geomagnetic reversal time scale on estimates of current plate motions, *Geophys. Res. Lett.*, *21*, 2191–2194, doi:10.1029/94GL02118.

Elgueta, S., and R. Arcos (1994), *Geología y Modelo de Sedimentación de la Secuencia Cretácico Terciaria de la Cuenca de Arauco*, 34 pp., Empresa Nac. del Petróleo, Santiago.

Encinas, A., et al. (2008), Rapid and major coastal subsidence during the late Miocene in south-central Chile, *J. South Am. Earth Sci.*, *25*, 157–175, doi:10.1016/j.jsames.2007.07.001.

Engdahl, E. R., and A. Villaseñor (2002), Global seismicity: 1900–1999, in *International Handbook of Earthquake and Engineering Seismology*, edited by W. H. Lee et al., pp. 665–690, Academic, Amsterdam.

Farías, M., et al. (2008), Late Miocene high and rapid surface uplift and its erosional response in the Andes of central Chile (33°–35°S), *Tectonics*, *27*, TC1005, doi:10.1029/2006TC002046.

Farr, T. G., et al. (2007), The shuttle radar topography mission, *Rev. Geophys.*, *45*, RG2004, doi:10.1029/2005RG000183.

Finger, K. L., S. N. Nielsen, T. J. DeVries, A. Encinas, and D. E. Peterson (2007), Paleontologic evidence for sedimentary displacement in Neogene fore-arc basins of central Chile, *Palaios*, *22*, 3–16, doi:10.2110/palo.2005.p05-081r.

Fitzgerald, P. G., E. Stump, and T. F. Redfield (1993), Late Cenozoic uplift of Denali and its relation to relative plate motion and fault morphology, *Science*, *259*, 497–500, doi:10.1126/science.259.5094.497.

Folguera, A., V. A. Ramos, and D. Melnick (2002), Transición de los Andes Patagónicos a los Andes centrales: Extremo norte del sistema de Liquiñe-Ofqui (38°S), *Rev. Geol. Chile*, *29*, 227–240.

Forsythe, R., and E. Nelson (1985), Geological manifestations of ridge collision: Evidence from the Golfo de Penas-Taitao basin, southern Chile, *Tectonics*, *4*, 477–495, doi:10.1029/TC004i005p00477.

Freed, A. M. (2005), Earthquake triggering by static, dynamic, and postseismic stress transfer, *Annu. Rev. Earth Planet. Sci.*, *33*, 335–367, doi:10.1146/annurev.earth.33.092203.122505.

Glodny, J., et al. (2005), Internal dynamics of a paleoaccretionary wedge: Insights from combined isotope tectonochronology and sandbox modelling of the south-central Chilean fore-arc, *Earth Planet. Sci. Lett.*, *231*, 23–39, doi:10.1016/j.epsl.2004.12.014.

Glodny, J., et al. (2008a), Differential late Paleozoic active margin evolution in south-central Chile (37°S–40°S): The Lanalhue fault zone, *J. South Am. Earth Sci.*, *26*, 397–411, doi:10.1016/j.jsames.2008.06.001.

Glodny, J., K. Gräfe, H. Echtler, and M. Rosenau (2008b), Mesozoic to Quaternary continental margin dynamics in south-central Chile (36–42°S): The apatite and zircon fission track perspective, *Int. J. Earth Sci.*, *97*, 1271–1291, doi:10.1007/s00531-007-0203-1.

González, E. (1990), Hydrocarbon resources in the coastal zone of Chile, in *Geology of the Andes and Its Relation to Hydrocarbon and Mineral Resources*, edited by G. E. Ericksen et al., pp. 383–404, Cricum-Pac. Counc. for Energy and Miner. Resour., Houston, Tex.

Granger, D. E., and P. F. Muzikar (2001), Dating sediment burial with in situ-produced cosmogenic nuclides: Theory, techniques, and limitations, *Earth Planet. Sci. Lett.*, *188*, 269–281, doi:10.1016/S0012-821X(01)00309-0.

Granger, D. E., and A. L. Smith (2000), Dating buried sediments using radioactive decay and muogenic production of ^{26}Al and ^{10}Be, *Nucl. Instrum. Methods Phys. Res. Sect. B*, *172*, 822–826, doi:10.1016/S0168-583X(00)00087-2.

Groß, K., et al. (2008), The reflection seismic survey of project TIPTEQ: The inventory of the Chilean subduction zone at 38.2°S, *Geophys. J. Int.*, *172*, 565–571.

Haberland, C., A. Rietbrock, D. Lange, K. Bataille, and S. Hofmann (2006), Interaction between fore-arc and oceanic plate at the south-central Chilean margin as seen in local seismic data, *Geophys. Res. Lett.*, *33*, L23302, doi:10.1029/2006GL028189.

Hackney, R., et al. (2006), The segmented overriding plate and coupling at the south-central Chilean Margin (36–42°S), in *The Andes: Active Subduction Orogeny*, edited by O. Oncken et al., pp. 355–374, Springer-Verlag, Berlin.

Hanks, T., and H. Kanamori (1979), A moment magnitude scale, *J. Geophys. Res.*, *84*, 2348–2350, doi:10.1029/JB084iB05p02348.

Hearty, P. J., and P. Kindler (1995), Sea-level highstand chronology from stable carbonate platforms (Bermuda and the Bahamas), *J. Coastal Res.*, *11*, 675–689.

Hervé, F. (1988), Late Paleozoic subduction and accretion in southern Chile, *Episodes*, *11*, 183–188.

Hervé, F. (1994), The southern Andes between 39° and 44°S latitude: The geological signature of a transpressive tectonic regime related to a magmatic arc, in *Tectonics of the Southern Central Andes*, edited by K. J. Reutter et al., pp. 243–248, Springer, Berlin.

Hyndman, R. D., and K. Wang (1995), The rupture zone of Cascadia great earthquakes from current deformation and the thermal regime, *J. Geophys. Res.*, *100*, 22,133–22,154, doi:10.1029/95JB01970.

Johnson, M. E., and L. K. Libbey (1997), Global review of upper pleistocene (Substage 5e) rocky shores: Tectonic segregation, substrate variation, and biological diversity, *J. Coastal Res.*, *13*, 297–307.

Johnson, S. Y., R. J. Blakely, W. J. Stephenson, S. V. Dadisman, and M. A. Fisher (2004), Active shortening of the Cascadia fore-arc and implications for seismic hazards of the Puget Lowland, *Tectonics*, *23*, TC1011, doi:10.1029/2003TC001507.

Kaizuka, S., T. Matsuda, M. Nogami, and N. Yonekura (1973), Quaternary tectonic and recent seismic crustal movements in the Arauco peninsula and its environs, central Chile, *Geogr. Rep. Tokyo Metrop. Univ.*, *8*, 1–49.

Kanamori, H. (1977), The energy release in great earthquakes, *J. Geophys. Res.*, *82*, 2981–2987, doi:10.1029/JB082i020p02981.

Kelleher, J. A. (1972), Rupture zones of large South American earthquakes and some predictions, *J. Geophys. Res.*, *77*, 2089–2103.

Keller, E. A., and N. Pinter (2002), *Active Tectonics: Earthquakes, Uplift, and Landscape*, Prentice-Hall, Upper Saddle River, N. J.

Kendrick, E., et al. (2003), The Nazca-South America Euler vector and its rate of change, *J. South Am. Earth Sci.*, *16*, 125–131, doi:10.1016/S0895-9811(03)00028-2.

Klotz, J., et al. (2001), Earthquake cycle dominates contemporary crustal deformation in central and southern Andes, *Earth Planet. Sci. Lett.*, *193*, 437–446, doi:10.1016/S0012-821X(01)00532-5.

Kodaira, S., et al. (2006), A cause of rupture segmentation and synchronization in the Nankai trough revealed by seismic imaging and numerical simulation, *J. Geophys. Res.*, *111*, B09301, doi:10.1029/2005JB004030.

Krawczyk, C., et al. (2006), Geophysical signatures and active tectonics at the south-central Chilean margin, in *The Andes: Active Subduction Orogeny*, edited by O. Oncken et al., pp. 171–192, Springer-Verlag, Berlin.

Kukla, G. J., et al. (2002), Last interglacial climates, *Quat. Res.*, *58*, 2–13, doi:10.1006/qres.2001.2316.

Lajoie, K. R. (1986), Coastal tectonics, in *Active Tectonics*, edited by R. E. Wallace, pp. 95–124, Natl. Acad. Press, Washington, D. C.

Lal, D. (1991), Cosmic ray labeling of erosion surfaces: In situ nuclide production rates and erosion models, *Earth Planet. Sci. Lett.*, *104*, 424–439, doi:10.1016/0012-821X(91)90220-C.

Lavenu, A., and J. Cembrano (1999), Compressional- and transpressional-stress pattern for Pliocene and Quaternary brittle deformation in fore-arc and intra-arc zones (Andes of central and southern Chile), *J. Struct. Geol.*, *21*, 1669–1691, doi:10.1016/S0191-8141(99)00111-X.

Le Roux, J. P., and S. Elgueta (1997), Paralic parasequences associated with Eocene sea-level oscillations in an active margin setting: Trihueco Formation of the Arauco basin, Chile, *Sediment. Geol.*, *110*, 257–276, doi:10.1016/S0037-0738(96)00086-3.

Llenos, A., and J. J. McGuire (2007), Influence of fore-arc structure on the extent of great subduction zone earthquakes, *J. Geophys. Res.*, *112*, B09301, doi:10.1029/2007JB004944.

Lohrmann, J., et al. (2006), Subduction channel evolution in brittle fore-arc wedges: A combined study with scaled sandbox experiments, seismological and reflection seismic data and geological field evidence, in *The Andes: Active Subduction Orogeny*, edited by O. Oncken et al., pp. 237–262, Springer-Verlag, Berlin.

Lomnitz, C. (1970), Major earthquakes and tsunamis in Chile during the period 1535 to 1955, *Geol. Rundsch.*, *59*, 938–960, doi:10.1007/BF02042278.

Lomnitz, C. (2004), Major earthquakes of Chile: A historical survey, 1535–1960, *Seismol. Res. Lett.*, *75*, 368–378.

Lüth, S., et al. (2003), A crustal model along 39°S from a seismic refraction profile-ISSA 2000, *Rev. Geol. Chile*, *30*, 83–94.

Marquardt, C., A. Lavenu, L. Ortlieb, E. Godoy, and D. Comte (2004), Coastal neotectonics in southern central Andes: Uplift and deformation of marine terraces in northern Chile (27°S), *Tectonophysics*, *394*, 193–219, doi:10.1016/j.tecto.2004.07.059.

McCaffrey, R. (1992), Oblique plate convergence, slip vectors, and fore-arc deformation, *J. Geophys. Res.*, *97*, 8905–8915, doi:10.1029/92JB00483.

McCaffrey, R., et al. (2007), Fault locking, block rotation and crustal deformation in the Pacific Northwest, *Geophys. J. Int.*, *169*, 1315–1340, doi:10.1111/j.1365-246X.2007.03371.x.

Melnick, D., and H. P. Echtler (2006a), Inversion of fore-arc basins in south-central Chile caused by rapid glacial age trench fill, *Geology*, *34*, 709–712, doi:10.1130/G22440.1.

Melnick, D., and H. P. Echtler (2006b), Morphotectonic and geologic digital map compilations of the south-central Andes (36°–42°(S), in *The Andes: Active Subduction Orogeny*, edited by O. Oncken et al., pp. 565–568, Springer-Verlag, Berlin.

Melnick, D., B. Bookhagen, H. Echtler, and M. Strecker (2006a), Coastal deformation and great subduction earthquakes, Isla Santa María, Chile (37°S), *Geol. Soc. Am. Bull.*, *118*, 1463–1480, doi:10.1130/B25865.1.

Melnick, D., F. Charlet, H. P. Echtler, and M. De Batist (2006b), Incipient axial collapse of the Main Cordillera and strain partitioning gradient between the central and Patagonian Andes, Lago Laja, Chile, *Tectonics*, *25*, TC5004, doi:10.1029/2005TC001918.

Mogi, K. (1979), Two kinds of seismic gaps, *Pure Appl. Geophys.*, *117*, 1172–1186, doi:10.1007/BF00876213.

Moreno, M. S., J. Klotz, D. Melnick, H. Echtler, and K. Bataille (2008), Active faulting and heterogeneous deformation across a megathrust segment boundary from GPS data, south-central Chile (36°–39°S), *Geochem. Geophys. Geosyst.*, *9*, Q12024, doi:10.1029/2008GC002198.

Mpodozis, C., and V. Ramos (1990), The Andes of Chile and Argentina, in *Geology of the Andes and Its Relation to Hydrocarbon and Mineral Resources*, edited by G. E. Ericksen et al., pp. 59–90, Cricum-Pac. Counc. for Energy and Miner. Resour., Houston, Tex.

Muhs, D. R. (2002), Evidence for the timing and duration of the last interglacial period from high-precision uranium-series ages of corals on tectonically stable coastlines, *Quat. Res.*, *58*, 36–40, doi:10.1006/qres.2002.2339.

Muhs, D. R., K. R. Simmons, and B. Steinke (2002), Timing and warmth of the Last Interglacial period: New U-series evidence from Hawaii and Bermuda and a new fossil compilation for North America, *Quat. Sci. Rev.*, *21*, 1355–1383, doi:10.1016/S0277-3791(01)00114-7.

Nelson, R., and W. Manley (1992), Holocene coseismic and aseismic uplift of the Isla Mocha, south-central Chile, *Quat. Int.*, *15–16*, 61–76, doi:10.1016/1040-6182(92)90036-2.

Nielsen, S. N., and C. Valdovinos (2008), Mollusks of the Tubul Formation (south-central Chile): Implications for the early Pleistocene climate of the southeastern Pacific, *Nautilus*, *122*, 201–216.

Pineda, V. (1986), Evolución paleográfica de la cuenca sedimentaria Cretácico-Terciaria de Arauco, in *Geología y Recursos Minerales de Chile*, edited by J. Frutos et al., pp. 375–390, Univ. de Concepción, Concepción, Chile.

Plafker, G., and J. C. Savage (1970), Mechanism of the Chilean earthquake of May 21 and 22, 1960, *Geol. Soc. Am. Bull.*, *81*, 1001–1030, doi:10.1130/0016-7606(1970)81[1001:MOTCEO]2.0.CO;2.

Radic, J. P., P. Alvarez, and L. Rojas (2005), Tectonostratigraphic evolution of the Arauco-Itata fore-arc basin, central Chile, paper presented at 6th International Symposium of Andean Geodynamics, Inst. de Rech. pour le Dev., Barcelona, Spain.

Ramsay, J. G., and M. I. Huber (1987), *The Techniques of Modern Structural Geology: Folds and Fractures*, Academic, London.

Ranero, C. R., R. von Huene, W. Weinrebe, and C. Reichert (2006), Tectonic processes along the Chile convergent margin, in *The Andes: Active Subduction Orogeny*, edited by O. Oncken et al., pp. 92–121, Springer-Verlag, Berlin.

Rehak, K., M. R. Strecker, and H. P. Echtler (2008), Morphotectonic segmentation of an active fore-arc, 37°–41°S, Chile, *Geomorphology*, *94*, 98–116, doi:10.1016/j.geomorph.2007.05.002.

Reichert, C., et al. (2002), Fahrtbericht Sonne-Fahrt SO-161 Leg 2 & 3, SPOC: Subduktionsprozesse vor Chile, *Forschungsvorhaben 03G0161A*, Bundesanst. für Geowiss. und Rohstoffe, Hannover, Germany.

Robinson, D. P., S. Das, and A. B. Watts (2006), Earthquake rupture stalled by a subducting fracture zone, *Science*, *312*, 1203–1205, doi:10.1126/science.1125771.

Rosenau, M., D. Melnick, and H. Echtler (2006), Kinematic constraints on intra-arc shear and strain partitioning in the southern Andes between 38°S and 42°S latitude, *Tectonics*, *25*, TC4013, doi:10.1029/2005TC001943.

Ruff, L. J. (1989), Do trench sediments affect great earthquake occurrence in subduction zones?, *Pure Appl. Geophys.*, *129*, 263–282, doi:10.1007/BF00874629.

Satake, K., and B. F. Atwater (2007), Long-term perspectives on giant earthquakes and tsunamis at subduction zones, *Annu. Rev. Earth Planet. Sci.*, *35*, 349–374, doi:10.1146/annurev.earth.35.031306.140302.

Scholz, C. H. (2002), *The Mechanics of Earthquakes and Faulting*, 2nd ed., 471 pp., Cambridge Univ. Press, Cambridge, U. K.

Seivers, A. (1963), The seismic sea wave of 22 May 1960 along the Chilean coast, *Bull. Seismol. Soc. Am.*, *53*, 1125–1190.

Sernageomin (2003), Geologic map of Chile: Digital version, scale 1:1.000.000, Santiago, Chile.

Shackleton, N. J., and N. D. Opdyke (1973), Oxygen isotope and paleomagnetic stratigraphy of the equatorial Pacific cores V28–238: Oxygen isotope and ice volumen on as 10^5 years and 10^6 years scale, *Quat. Res.*, *3*, 39–55, doi:10.1016/0033-5894(73)90052-5.

Shackleton, N. J., A. Berger, and W. R. Peltier (1990), An alternative astronomical calibration of the lower Pleistocene timescale based on ODP Site 677, *Trans. R. Soc. Edinburgh Earth Sci.*, *81*, 251–261.

Shimazaki, K., and T. Nakata (1980), Time-predictable recurrence model for large earthquakes, *Geophys. Res. Lett.*, *7*, 279–282, doi:10.1029/GL007i004p00279.

Somoza, R. (1998), Updated Nazca (Farallon)-South America relative motions during the last 40 My: Implications for mountain building in the central Andean region, *J. South Am. Earth Sci.*, *11*, 211–215, doi:10.1016/S0895-9811(98)00012-1.

Song, T. R. A., and M. Simons (2003), Large trench-parallel gravity variations predict seismogenic behavior in subduction zones, *Science*, *301*, 630–633, doi:10.1126/science.1085557.

Suárez, M., and C. Emparán (1997), Hoja Curacautín: Regiones de la Araucanía y del Bío-Bío, *Map 105*, scale scale1:250,000/scale, Serv. Nac. de Geol. y Minería, Santiago, Chile.

Tassara, A., H. J. Götze, S. Schmidt, and R. Hackney (2006), Three-dimensional density model of the Nazca plate and the Andean continental margin, *J. Geophys. Res.*, *111*, B09404, doi:10.1029/2005JB003976.

Tassara, A., C. Swain, R. Hackney, and J. Kirby (2007), Elastic thickness structure of South America estimated using wavelets and satellite-derived gravity data, *Earth Planet. Sci. Lett.*, *253*, 17–36, doi:10.1016/j.epsl.2006.10.008.

Taylor, F., C. Frohlich, J. Lecolle, and M. Strecker (1987), Analysis of partially emerged corals and reef terraces in the central Vanuatu arc: Comparison of contemporary coseismic and nonseismic with Quaternary vertical movements, *J. Geophys. Res.*, *92*, 4905–4933, doi:10.1029/JB092iB06p04905.

Tebbens, S. F., and S. C. Cande (1997), Southeast Pacific tectonic evolution from early Oligocene to present, *J. Geophys. Res.*, *102*, 12,061–12,084, doi:10.1029/96JB02582.

Thackray, G. D. (1998), Convergent-margin deformation of Pleistocene strata on the Olympic coast of Washington, USA, *Geol. Soc. Spec. Publ.*, *146*, 199–211.

Thatcher, W. (1990), Order and diversity in modes of Circum-Pacific earthquake recurrence, *J. Geophys. Res.*, *95*, 2609–2624, doi:10.1029/JB095iB03p02609.

Thomson, S. N. (2002), Late Cenozoic geomorphic and tectonic evolution of the Patagonian Andes between latitudes 42°S and 46°S: An appraisal based on fission-track results from the transpressional intra-arc Liquiñe-Ofqui fault zone, *Geol. Soc. Am. Bull.*, *114*, 1159–1173.

Thornburg, T. M., L. D. Kulm, and D. M. Hussong (1990), Submarine-fan development in the southern Chile trench: A dynamic interplay of tectonics and sedimentation, *Geol. Soc. Am. Bull.*, *102*, 1658–1680, doi:10.1130/0016-7606(1990)102<1658:SFDITS>2.3.CO;2.

Völker, D., et al. (2006), Latitudinal variation in sedimentary processes in the Peru-Chile trench off central Chile, in *The Andes: Active Subduction Orogeny*, edited by O. Oncken et al., pp. 193–216, Springer-Verlag, Berlin.

Wang, K., et al. (2007), Crustal motion in the zone of the 1960 Chile earthquake: Detangling earthquake-cycle deformation and fore-arc-sliver translation, *Geochem. Geophys. Geosyst.*, *8*, Q10010, doi:10.1029/2007GC001721.

Wells, D. L., and K. J. Coppersmith (1994), New empirical relationships among magnitude, rupture length, rupture width, rupture area, and surface displacement, *Bull. Seismol. Soc. Am.*, *84*, 974–1002.

Wells, R. E., C. S. Weaver, and R. J. Blakely (1998), Fore-arc migration in Cascadia and its neotectonic significance, *Geology*, *26*, 759–762, doi:10.1130/0091-7613(1998)026<0759:FAMICA>2.3.CO;2.

Wells, R. E., R. J. Blakely, Y. Sugiyama, D. W. Scholl, and P. A. Dinterman (2003), Basin-centered asperities in great subduction zone earthquakes: A link between slip, subsidence, and subduction erosion, *J. Geophys. Res.*, *108*(B10), 2507, doi:10.1029/2002JB002072.

Yáñez, G., J. Cembrano, M. Pardo, C. Ranero, and D. Selles (2002), The Challenger-Juan Fernández-Maipo major tectonic transition of the Nazca-Andean subduction system at 33–34°S: Geodynamic evidence and implications, *J. South Am. Earth Sci.*, *15*, 23–38, doi:10.1016/S0895-9811(02)00004-4.

————————

B. Bookhagen, Department of Geological and Environmental Sciences, Stanford University, 450 Serra Mall, Braun Hall, Building 320, Stanford, CA 94305, USA.

H. P. Echtler, GeoForschungsZentrum Potsdam, Telegrafenberg, D-14473 Potsdam, Germany.

D. Melnick and M. R. Strecker, Institut für Geowissenschaften, Universität Potsdam, Karl-Liebknecht-Strasse 24, Haus 27, D-14415 Potsdam, Germany. (melnick@geo.uni-potsdam.de)